UNIVERSIDADE DE LISBOA
FACULDADE DE CIÊNCIAS
DEPARTAMENTO DE FÍSICA

LET- and Radiation Quality-dependence of the complexity of DNA damages

João de Figueiredo Canhoto

Mestrado Integrado em Engenharia Física

Dissertação orientada por:
Prof. Luís Peralta
Prof. Ana Belchior

2018

I have no special talent. I am only passionately curious.

— Albert Einstein

Acknowledgments

My five-year journey as a college student in Portugal is now reaching its end, is now time to take some time to relax and be grateful for some moments and to some persons.

To my mentors, Prof. Ana, Hans and Uli, for believing in me and on my capacities as a student, as a person and as a future engineer. The last five months were rough and full of work and problems, but we ”constructed” this final project of which I am proud.

To Christa and Volker, for accepting me into their home and being one of the nicest couples I have ever met. It was a pleasure to meet both of you and your family. I will always remember your kindness. I truly believe that one day we will meet again.

To Elisa and Quentin, my latin gang!! Every time I remember my time in Germany, you are there. You helped me in ways I can't even describe. You were there in the good moments and you were there in the bad ones too. You heard me complain over and over again, but you always had something nice and helpful to say, something that helped me stay focused and motivated through the harshest of times. My time in Germany would not be the same without you. So I now thank you for everything! It was fantastic to get to know you, hang out with you and build this friendship that I will always cherish, and I know we will meet again in the future, that's for sure! I wish you the best of luck ever and you can count on me whenever you need.

E agora em Português....

À Rita, à Soraia e à Sara... não só pelos últimos cinco meses, mas pelos últimos cinco anos. Vivemos momentos que sempre me irei lembrar com um sorriso. A vossa amizade foi um elemento fundamental nesta aventura e será algo que sempre irei guardar para o futuro. Mesmo que não queiram, vão ter de me aguentar! Sou lapa mesmo.

Ao João... que apareceu já perto do final e mesmo assim conseguiu ganhar um destaque. Errado: não conseguiste, mereceste e muito. Por seres a pessoa que és e por teres dado o apoio que deste nos dias mais difíceis deste trabalho. Pela tua presença, que mesmo de longe, foi um porto de abrigo e conforto, e pela tua ajuda e disponibilidade: marcantes e extremamente importantes. No passado e presente a tua marca já é visível, não só neste trabalho. Do futuro pode-se não falar, mas eu sei o que desejo para ele e o quanto quero que estejas envolvido.

À Reitoria da Universidade de Lisboa, que no âmbito do programa Erasmus+, ajudou substancialmente a que este trabalho fosse possível de ser realizado e concluído.

E por fim, à família, aos pais. Pelos sacrifícios que fizeram durante 23 anos e que em tudo contribuíram para que hoje este trabalho e este curso estejam completos. Posso não mostrar a gratidão que sinto, mas está cá e o que fizeram é reconhecido e admirado.

To all these people and many more, I am here thanks to all of you. I am who I am because I had the

opportunity to know you, to live with you and to grow with you. For better or for worse, you all took part in my life. No matter how small the contribution was, it helped me to grow as a person and become the young adult you now see; it helped me to understand what my goals were and are; it helped to become stronger and smarter. It helped me, period.

MUITO OBRIGADO!

THANK YOU VERY MUCH!

VIELEN DANKE!

Resumo

Esta tese aborda o estudo dos efeitos biológicos induzidos por exposição à radiação-alfa (α) em células endoteliais da veia umbilical humana (HUVEC) e por exposição às radiações alfa e gama (γ) em células saudáveis (não cancerígenas) da próstata humana (RWPE-1).

A radiação ionizante pode interagir de duas formas com o DNA (o principal alvo da radiação ionizante): diretamente, ao quebrar as ligações dos pares de bases da cadeia de DNA, ou indiretamente, ao quebrar as ligações de moléculas de água envolventes dando origem a radicais livres que podem interagir com a molécula de DNA. Existem vários tipos de danos, entre eles danos de base (*base damage*) ou *single-strand breaks*, mas os mais graves são os *double-strand breaks* (DSBs), isto é, quando a radiação é capaz de quebrar as ligações de dois pares de bases (pb, ou, em inglês, bp, *base pairs*), no mínimo, que distam a 10 bp ou menos e em cadeias opostas. Estas quebras podem resultar na clivagem da molécula de DNA e a célula pode não conseguir repará-las, dando a origem a mutações ou outros efeitos biológicos graves. Quando existe um DSB numa molécula de DNA, começa a existir um aglomerado de proteínas reparadoras nessa zona, proteínas essas que podem ser marcadas com marcadores florescentes e, posteriormente, serem observadas com a técnica de microscopia de florescência como focos (pequenos objetos circulares fluorescentes). Numa altura em que a radioterapia está a ganhar cada vez mais interesse e terreno nas opções de tratamento contra o cancro, é importante perceber como diferentes radiações causam danos nas moléculas de DNA.

Numa primeira parte, fez-se um estudo estatístico de dados recolhidos numa experiência levada a cabo em 2014, no PTB, realizado pelos orientadores. Nesta experiência células HUVEC foram expostas a radiação alfa de várias energias (8, 10 e 20 MeV) e a protões de 3 MeV. O PTB possui um sistema de microfeixe capaz de controlar o número de partículas emitido e o local onde são emitidas, dado a possibilidade de atingir diretamente o núcleo das células, em contrapartida aos *broadbeam*, que irradiam toda a área exposta. Desta maneira podemos controlar o número de focos que esperamos observar em fluorescência. Após uma etapa de reconhecimento das células, cada núcleo reconhecido foi exposto a 5 partículas do tipo de radiação em causa, no padrão quincunce (semelhante ao lado 5 de um dado). Após a radiação, seguiu-se o protocolo do ensaio de focos (*Foci Assay*). O objetivo deste estudo passou por tentar obter, para cada qualidade de radiação, uma estimativa para a probabilidade de uma partícula dessa radiação induzir um dano na cadeia de DNA. Para tal, as células expostas foram fotografadas com recurso a uma câmara acoplada a um microscópio de fluorescência e as imagens foram analisadas pelo *software CellProfiler* para identificação dos núcleos e do número de focos em cada um deles, bem como outras características de cada objeto, como intensidade e área. Os dados foram simulados como uma convolução entre uma função $I(k)$ que representa os focos induzidos por radiação e uma função $B(k)$, que representa os focos de *background* (devidos a manuseamento, stress, entre outras razões biológicas).

Numa primeira abordagem verificou-se que $B(k)$ seguia uma distribuição de decaimento exponencial, no entanto os processos básicos de limpeza de dados resultavam num ajuste fraco. Assim sendo, e como conhecer a função $B(k)$ ou estimá-la corretamente é importante, o foco desta parte passou a ser encontrar a melhor função de ajuste $B(k)$ aos dados aplicando valores limiares a parâmetros intrínsecos aos objetos como a intensidade total dos focos e a área dos núcleos. No que diz respeito à intensidade dos focos, aplicou-se valores limites entre 0 e 100. Em cada situação, focos com intensidade inferior ao limite eram descartados dos dados e procedeu-se ao ajuste de uma função de decaimento exponencial com parâmetros a (amplitude) e b (argumento da exponencial). Os ajustes foram comparados usando o teste do chi-quadrado *Goodness of Fit*. Neste teste os valores reais e obtidos pela função são comparados e o ajuste que apresenta o menor valor de chi-quadrado representa o melhor ajuste aos dados. Para a intensidade dos focos, verificou-se que o limite de 23 era o parâmetro ótimo (χ^2 = 0.070), registando uma melhoria em relação à situação em que nenhum limite é aplicado (χ^2 = 0.124). No passo seguinte, focámo-nos na área dos núcleos. Após observar a distribuição desta variável, escolheu-se três limites inferiores (4000, 7000 e 9000 pxl^2) e três superiores (16000, 18000 e 21000 pxl^2) e testou-se todas as combinações. O par de limites 7000/21000 (χ^2 = 0.0044) foi o que apresentou a maior melhoria no ajuste. Apesar da melhoria significativa na função $B(k)$ e também numa notável melhoria na função de ajuste $I(k)$, uma sobreposição linear de três binomiais de parâmetro p (probabilidade de induzir um dano), verificou-se que os parâmetros ótimos para os dados de *background* não são os mesmos para os dados de células irradiadas, pelo que o processo de limpeza destes últimos necessita de ser revisto no futuro.

A segunda parte do trabalho tinha como objetivo avaliar o *Relative Biological Effectiveness* (RBE) de protões na linha celular RWPE-1, células saudáveis epiteliais da próstata humana, através do Ensaio Clonogénico. O cancro da próstata é tratado mundialmente com recurso à radioterapia, sendo os protões a radiação escolhida, pelo que é importante averiguar qual a resposta das células saudáveis, que são circundantes às células cancerígenas, a esta radiação. Devido a problemas experimentais e questões de calendário, não foi possível realizar a experiência usando um feixe de protões, pelo que se optou por fazer um estudo usando a fonte radioativa Amerício-241, emissora de partículas alfa. Um grupo de células foi exposto a 0.5, 1, 2, 4, 6 e 10 Gy de fotões de Cobalto-60 e um segundo grupo foi exposto a 0.25, 0.5, 1 e 2 Gy de partículas alfa de Am-241. Para os fotões, sendo uma radiação pouco ionizante, usou-se o Modelo Linear Quadrático para se obter um ajuste aos dados, com resultados $\alpha_\gamma = 0.47 \pm 0.01$ Gy^{-1} e $\beta_\gamma = 0.006 \pm 0.001$ Gy^{-2}. Para as partículas alfa, usou-se o Modelo Linear, obtendo-se o parâmetro $\alpha = 1.13 \pm 0.02$ Gy^{-2}. O valor de RBE obtido, para uma fração de sobrevivência de 10%, para a radiação alfa emitida pela fonte de Amerício-241 foi de 2.27 ± 0.06. Este valor encontra-se longe de outros valores reportados por outras equipas, embora a comparação com estes não seja 100% correta,

uma vez que o RBE depende não só da radiação escolhida, como da radiação de referência (no nosso caso foi fotões de Co-60, nos outros usou-se Raios-X ou Cs-137) e, ainda mais importante, a linha celular usada. Sentiram-se ainda alguns problemas experimentais que poderão ter afetado o resultado final, uma vez que não foi possível recolher dados suficientes para inferir valores estatisticamente válidos.
Em conclusão, os objetivos iniciais desta tese não foram alcançados, mas o trabalho realizado abre portas para uma futura discussão de como analisar dados provenientes de um ensaio de focos, acentuando a importância de corretamente separar os dados obtidos, tentando ao máximo selecionar apenas os dados que são realmente relevantes para a análise. Relativamente ao segundo estudo, mantém-se ainda de grande interesse avaliar a resposta de células saudáveis da próstata aos protões, não só porque é importante registar a possível letalidade, como a falta de dados para esta linha celular pode tornar o tratamento perigoso.

Palavras-chave: focos induzidos por radiação, ensaio clonogénico, radioterapia, dosimetria, estatística

Abstract

This thesis addresses the study of the biological effects induced by ionising radiation, such as alpha-particles, photons and protons, in Human Umbilical Vein Endothelial cells (HUVEC) and normal (non-cancerous) human epithelial prostate cells (RWPE-1).

In the first part of the thesis, we aimed to obtain an estimative of the probability that different radiation qualities have in inducing DNA damage. HUVEC cells were exposed to 8, 10 and 20 MeV alpha-particles and 3 MeV protons in the microbeam facility at Physikalisch-Technische Bundesanstalt (PTB), Braunschweig, Germany, in a quincunx pattern (face-5 of a dice) so that each focus could be easily distinguished. For each radiation type, cells were imaged in a fluorescence microscope and the images of nuclei containing foci were analysed using the free software CellProfiler (CP) for identification and counting of nuclei and foci per nucleus. The data retrieved from CP can be seen as a convolution between radiation-induced foci and background foci (foci already present in the cells due to handling, stress or other biological factors) and, therefore, we modulated the data as $D(k) = I(k) * B(k)$. The aim was to find $I(k)$, a linear superposition of binomial distributions of parameter p, that would best fit our data, p being the probability that the chosen radiation induces DNA damage. After our first try, where we found that the background data was better represented by an exponential decay rather than a Poisson distribution ($\chi^2_{Exp} = 0.124$ against $\chi^2_{Poisson} = 133526$ in the Goodness of Fit Test, where a small values represents a good agreement between the data and the function) we noticed that our current function $B(k)$ didn't reproduce correctly our real data, which is important. We turned our focus to the background data and the cleaning process, in order to obtain a more realistic function. Besides the basic cleaning steps (remove artefacts, cells with a high number of foci, due to division, and cells close to the border of the image) we studied the influence, on the resulting frequency distribution, of parameters such as foci intensity and nuclei area. We started by applying a threshold on the foci intensity (meaning, that focus with an intensity below the threshold would be eliminated from our data) from 0 to 100 and found that when applying a threshold of 23 the agreement between the values given by the function and our data improved ($\chi^2 = 0.0070$). The agreement gets even better ($\chi^2 = 0.0044$) when we applied upper and lower thresholds for the nuclei area, with the best threshold being 7000 and 21000 pxl^2 for lower and upper thresholds, respectively. Although our background function greatly improved, the fitting of the irradiated data was still not good, which shows that further improvements in the cleaning of the irradiated data is necessary before trying to fit the function.

In the second part of the thesis we used RWPE-1 cells (non-cancerous human epithelial prostate cells). The prostate cancer is highly treated with radiotherapy and the radiation of choice is protons, so it is important to assess the impact of this radiation on the healthy cells. For this purpose, we planned a clonogenic assay where we would exposed RWPE-1 cells to Co-60 photons (reference radiation) and 3

MeV protons to assess the RBE value of the latter. However, due to experimental problems, that was not possible to do. Since RBE also depends on the cell line, we decided to evaluate the RBE value for Am-241 α-particles. The cells were exposed to 0.5, 1, 2, 4,6 and 10 Gy of photons and 0.25, 0.5, 1 and 2 Gy of α-particles. The resulting RBE value was of 2.27 ± 0.06. This value was far from values reported by other teams around the world, although they used different cell lines and reference radiations.

Keywords: radiation-induced foci, clonogenic assay, radiotherapy, dosimetry, statistics

Contents

List of Tables

List of Figures

Chapter 1

Introduction and Outline

Ionizing radiation (IR) induces a wide variety of biological effects, mostly related with damages induced to the DNA molecule, the main target for radiation, since it holds crucial information for cell functioning and reproduction [1]. From the moment cells are exposed to radiation, there is a number of possible outcomes from no damages, passing by small damages easily repaired by cell's repair mechanisms, cell death and even cell mutations that may lead to cancer. However, the occurrence of these effects varies with the absorbed dose as well as with the radiation quality (i.e. type and energy), which is also determining damage complexity, and cell type and radiosensitivity.

Cell death (see Chapter 3 for definition of "death") may sound bad, but in some cases is something quite useful, for example in radiotherapy (RT) where cancer cells are targeted with ionizing radiations to stop their proliferation. Radiotherapy is obtaining an ever-growing fame and interest, specially the modality of particle and ion therapy that sees tumours being targeted by particles like protons and ions like carbon-ion, with many facilities around the world already in operation and some under construction or in planning stage [2] and Portugal getting a proton therapy facility by 2021 [3]. Proton has shown a relative more effectiveness comparing to the standard photon therapy (to this day, a value of 1.1 is being used in clinics) due to the physical properties of protons that allow one to reduce the dose to healthy tissues. However, it is currently known that the RBE values for protons slightly changes along the beam path, which can lead to a different dose distribution on the patient.

This dissertation aims to go a step further in the knowledge on biological effects of radiations and obtain not only relationships between DNA damages and Linear Energy Transfer (LET) for different radiation qualities, mainly the probability of inducing a damage on the DNA molecule, but also to assess some of the concerns of proton therapy using healthy cells from the human prostate.

1.1 Outline of Thesis and Work

1.1.1 Outline of Thesis

This dissertation describes the work performed at C^2TN and PTB during 5 months and it is divided in seven chapters: Chapter 2 - Radiation Physics, Therapy and Dosimetry - is a very brief but necessary chapter summarizing what is so well known about Radiation Physics, with a particular focus on some ionizing radiations. Following that there is a small introduction to radiation therapy, mainly proton therapy, presenting reasons why the work done is important. The third part consists of a quick guide to all dosimetric quantities that are important to have in mind during the reading of the present work.
In Chapter 3 - Radiobiology -, I start by briefly explaining what exactly radiation biology is and what are its aims. I then continue to explain some basic but essential concepts and radiobiological quantities for the present work.
Chapter 4 - Materials and Methods - introduces and explains the three different apparatuses used for irradiation, two of them from PTB (Germany) and the third one from C^2TN (Portugal). The second part of this chapter gives a quick, although somehow detailed, information on the protocol followed prior, during and after the irradiation day.
Chapter 5 - Results and Discussion - presents the results from the work performed, explains how the data was analysed and gives a brief discussion, comparing them to values found in literature and similar experiments.
Finally, Chapter 6 - Conclusion and Final Remarks - concludes this long project and gives insight into what may come ahead.

1.1.2 Outline of Work

This thesis is composed of, mainly, two topics very important to dosimetry and radiobiology: the probability of inducing damages in DNA, which will be helpful for future researches in many fields of expertise, and the RBE of protons for prostate cells, which is of high importance in radiotherapy.

Part One: Foci Analysis

To assess the probability of inducing a DNA damage, a specific cell line was exposed to different types of radiation and energies. The cell line chosen was HUVEC (Human Umbilical Vein Endothelial Cells) and they were exposed to α-particles of 8, 10 and 20 MeV (initial energy) and protons of 3 MeV. With different radiations and energies come different LET and, therefore, different track structures which lead to different yields of DNA damage. Looking from a macroscopic point of view, those yields depend on the LET of the radiation, therefore, if we analyse the yield of each radiation it may be possible to

estimate a probability of inducing a DNA damage depending on the radiation chosen and to get an idea of its behaviour with the LET when plotting the estimative against that macroscopic quantity. The goal of this study is to find a function (and the respective parameters) that closely fits the frequency distribution for irradiate cells and be able to indicate an estimative of the probability of inducing a DNA damage based on the radiation's LET.

Part Two: RBE of protons

For the second part, we aim to obtain the Relative Biological Effectiveness (RBE) of 3 MeV protons. As described before, the RBE is a way of comparing how damaging the radiation is comparing to a reference radiation (usually photons). For this purpose, we will perform 2 clonogenic assays: one with cells exposed to different doses of Cobalt-60 photons, to serve as the reference radiation, and the other with cells exposed to different doses of 3 MeV protons. After approximately two weeks, we can count the number of colonies formed for each of the doses and obtained the dose-response relationship for photons and protons for this cell line. Using equation 3.4 and the curve expressions that we will obtain, we can calculate the RBE value for protons and for this cell line.

Chapter 2

Radiation Physics, Therapy and Dosimetry

2.1 Radiation Physics

In physics, radiation is considered as the process of emission or transmission of energy through space or material medium and includes electromagnetic, particle, acoustic and gravitational radiations. For electromagnetic and particle radiation, depending on the energy of the radiated particles, the radiation can either be considered ionizing or non-ionizing. Ionizing radiation is the most problematic and focus of many studies since it carries enough energy to ionize atoms, molecules and break biological molecular bonds and so can be harmful to living organisms.
Common natural sources of ionizing radiations are radioactive materials that emit α, β and γ radiation and common anthropogenic sources are X-rays machines for medical purposes, for example.

Alpha radiation

Alpha radiation consists in the production and emission of α particles (Figure 2.1), nuclei of Helium-4, through a process called alpha decay. Usually α particles have energies of between 3 and 7 MeV. Due to their charge and large mass, they interact strongly with matter and are easily stopped (in air the range is of a few centimetres). Although they can't penetrate the outer layer of dead skin cells, they can cause serious cell damage as they are highly ionizing.

X- and Gamma-Radiation

Unlike alpha radiation, gamma radiation, or γ-ray (Figure 2.2), doesn't consist in an emission of a nuclear particle but rather in an emission of a photon. Photons are weightless and charge-less and, therefore, can travel longer than alpha particles and are less susceptible to matter interaction. They can only be attenuated with shields built with elements of a high atomic number, such as lead, and deposit less energy along their paths than alpha particles. Therefore, gamma radiation is considered sparsely

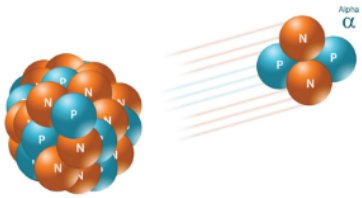

Figure 2.1: Pictorial representation of an α decay with an unstable nucleus emitting an α particle [Adapted from the Mirion Technologies website].

ionizing.

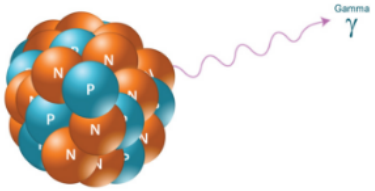

Figure 2.2: Pictorial representation of a γ radiation with an unstable nucleus emitting a photon [Adapted from the Mirion Technologies website].

X-rays are similar to gamma radiation, however, they originate from the electron cloud. X-rays have a longer wavelength and a lower energy than photons from γ-radiation.

2.2 Radiation Therapy

Radiation therapy is one of the standard methods for cancer treatment and is one of the most important and effective treatment modalities for all types of solid malignancies. According to [4], a total of 45% of all cancer patients is estimated to get cured and approximately 23% benefit from radiation therapy, either administrated alone or in combination with surgery or chemotherapy-immunotherapy. It started by using X-rays, but it quickly expanded to Co-60 sources and even high energy linear accelerators and cyclotrons, making it possible to treat cancers with a variety of particles (e.g. electrons and protons) and, more recently, ions. Nowadays, proton therapy is being seen as the optimal modality to deliver radiation therapy due to the properties of protons regarding the interaction with matter and energy deposition.
The proton's energy loss is given by the Bethe-Bloch equation which says that, in first order, the mean energy loss per distance travelled varies with the inverse squared speed ($dE/dx \propto 1/v^2$). This means that, when used in therapy, protons at high speed deliver little energy to the entrance tissues and a large amount of energy to a small, deep area (corresponding to a narrow peak called Bragg Peak), before quickly falling off, opposing the exponential decline that conventional photon radiations present (Figure

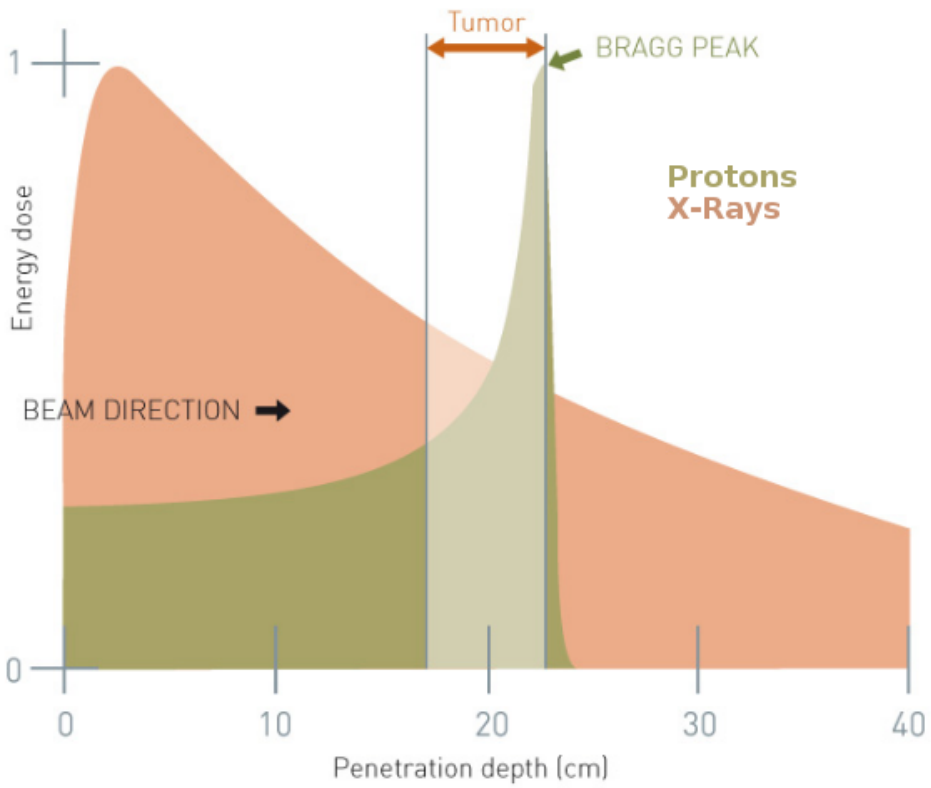

Figure 2.3: Comparison of the dose distribution along the penetration depth between X-rays and protons. [Adapted from the Rinecker Proton Therapy Center website].

2.3).

As it will be explained in chapter 3, one way to compare the effectiveness of different radiation qualities is by assessing the Relative Biological Effectiveness (RBE) for the test radiation. As of now, the clinical practised value of RBE for protons is 1.1, which means proton therapy is 10% more effective than the conventional photon therapy, since it spares the healthy tissues/cells surrounding the cancer. Even so, it is known that the RBE varies across the spread-out Bragg peak and proton therapy still delivers energy to healthy, normal tissues which may cause a future problem, therefore making important to assess the damages of protons on healthy tissues and the variation of the RBE.

2.3 Radiation Dosimetry

In order to study the effects of radiation not only in radiobiology but in every possible experiment where they are used, it is important to know (or how to calculate) certain parameters associated with the radiation source and the experimental setting. These parameters are called Dosimetric Quantities and they can depend on the quality and type of radiation, the time and distance of exposure, the source itself, among others.

In this section, I give a basic definition of the dosimetric quantities relevant to the work.

Absorbed Dose and Dose Rate

Absorbed dose is one of the fundamental quantities in Radiation Dosimetry and is defined as the ratio of the mean energy absorbed within a mass. Since the energy absorption is basically a stochastic process at a microscopic level, absorbed dose is considered a macroscopic quantity. Mathematically, absorbed dose is defined as the ratio between the mean energy imparted $d\bar{\varepsilon}$ over a mass dm, as given in the following equation, and has units of Joule per kilogram, also known as Gray (Gy).

$$D = \frac{d\bar{\varepsilon}}{dm} \tag{2.1}$$

ε is the energy imparted in an absorber of mass m.
Another important quantity is called the Dose rate defined as the absorbed dose per unit time and therefore has units of Gray per second (Gy/s). Dose rate ($\dot{D}$) is an important quantity since it has already been seen and proven that different dose rates give origin to different biological effects.

Liner Energy Transfer (LET)

Linear Energy Transfer, usually referred to as LET, indicates the amount of energy per path length that a charged particle transfers to the medium along its path through ionizations. Ionizing radiations that have a low density of interactions along the tracks are called low-LET radiations and considered sparsely ionizing. Conversely, if a radiation has a high density of ionizations along its track, it is considered as densely ionizing and called high-LET radiation (e.g. alpha particles). The common unit is $keV/\mu m$ (kiloelectron volt per micrometer) and, mathematically, LET is described by equation 2.2. Figure 2.4 shows the difference between low- and high-LET radiations.

$$LET = \frac{dE}{dx} \tag{2.2}$$

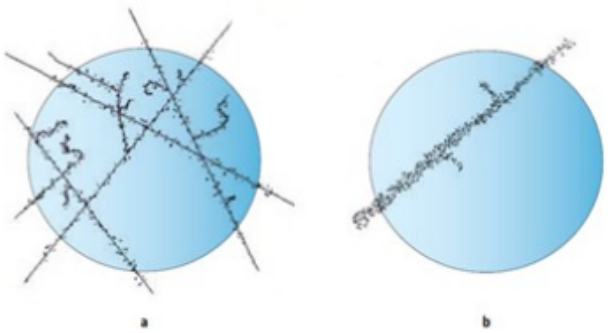

Figure 2.4: Schematic representation of low-(a) and high-LET (b) radiations, also known as sparsely and densely ionizing radiations, respectively [5].

Particle and Energy Fluence

When a radiation source is put in the vicinity of any object, that object will be exposed to a radiation field due to the emission of the source. In Radiation Dosimetry, a radiation field created by a source can be described by two quantities: particle fluence and energy fluence.

If we are interested in describing the field by the number of particles dN incident on a sphere of cross-sectional area dA, then we use the quantity called Particle Fluence which mathematically is given by equation 2.3 with units m^{-2}.

$$\Phi = \frac{dN}{dA} \tag{2.3}$$

On the other hand, a radiation field can also be described by Energy Fluence, [6], which can be calculated if we know both the particle fluence and the energy that each particle carries. It has units Jm^{-2} and, for monoenergetic particles, is given by equation 2.4, where R denotes the radiance (the product between the number of particles N and the particle energy E):

$$\Psi = \left(\frac{dN}{dA}\right) E = \Phi E = \frac{dR}{dA} \tag{2.4}$$

If we take these quantites per unit time, we have the particle and energy fluence rate which give, respectively, the amount of particles/energy per unit area dA per unit time dt and are given by the following expressions:

$$\dot{\Phi} = \frac{dN}{dAdt} \tag{2.5}$$

$$\dot{\Psi} = \left(\frac{dN}{dAdt}\right) E = \dot{\Phi} E = \frac{dR}{dAdt} \tag{2.6}$$

Chapter 3

Radiobiology

Radiation biology often referred to simply as radiobiology, is a branch of science that studies the effects of ionizing radiation (IR) on living organisms, combining the fields of physics and biology. The studies aim to understand and find a relationship between the biological effects in cells (or parts of them) due to energy absorption. This relationship is not easy to assess since there are many factors, such as Linear Energy Transfer (LET), dose distribution, radiosensitivity, etc.

DNA damage

Nowadays it is clear that the main target for inducing radiation effects is the DNA (deoxyribonucleic acid) molecule [7]. During exposure to ionizing radiation, either charged or uncharged particles, x-rays or γ-rays, radiation can be absorbed (through the usual physical effects between radiation and atoms/molecules), which may lead to later biological damages. If the radiation interacts directly with critical targets in the cell, those targets may be ionized or excited through Coulomb interactions, which gives rise to a chain of physical and chemical events that may produce biological damages (breaks in one or both the strands of the DNA double helix structure). This is called the direct action of ionizing radiation (Figure 3.1, bottom) and it is the dominant process for high LET particles. However, those breaks can also be caused by the interaction between the DNA molecule and free radicals, the indirect action (Figure 3.1, top) of ionizing radiation. Since 80% of the cell is water, radiation can interact with those water molecules instead and produce free radicals like H_2O^+ or OH$\bullet$ which in turn can cause damages to the targets. Two-thirds of the damages produced by low LET radiation is due to the indirect action.
Ionizing radiation induces a wide number of lesions in DNA, most of them easily repaired by the cell, among them base damage, single-strand break (SSB) and double-strand break (DSB). SSBs represent damages in nucleotides in one of the two strands of the double helix molecule. They don't have an important biological consequence since they are easily repaired through many repair mechanisms where the damaged nucleotide is replaced with an undamaged one. On the other hand, if radiation causes two

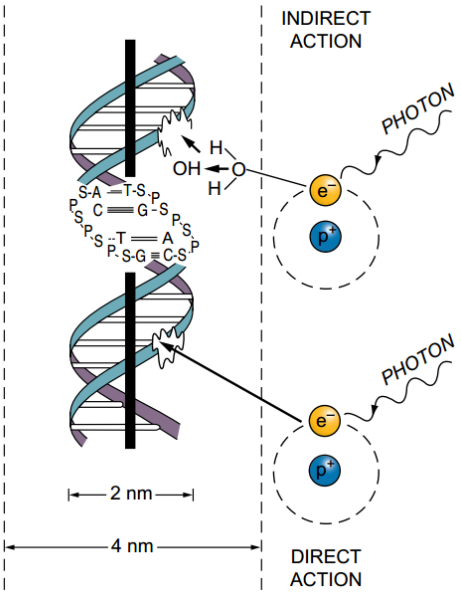

Figure 3.1: Schematic illustration of direct (bottom) and indirect (top) actions of radiation. Direct effects happen when radiation directly interacts with the DNA molecule whereas indirect effects occur when radiation interacts with a water molecule, for example, producing a hydroxil radical which, in turn, interacts with the DNA molecule [7].

damages each in one of the strands and they are directly opposed or separated by a few base pairs (bp), usually up to 10 bp, we are facing a DSB, which may cause the cleavage of chromatin in two pieces and, depending on the severity, may result in cell killing, carcinogenesis or mutation.

Assessing DNA damage

Although it is known that radiation can cause damages to the DNA molecule, it is still important to assess and quantify those damages, or rather their consequences, and relate them to physical dosimetric quantities (such as Dose or LET) in order to establish a relationship of cause-effect.

One of the common cause-effect relationships is the dose-survival fraction relationship (or Cell Survival Curve, addressed in subsection 3.1.1) which can be obtained by performing a Clonogenic Assay. This technique consists in plating cells over multiple dishes that are irradiated with different nominal doses. After irradiation, cells are incubated and allowed to grow into macroscopic colonies (colonies with more than 50 cells). The technique is addressed in section 3.1 with more details.

Among the many techniques that have been used over the years to measure DNA strand breaks, the Radiation-induced Foci Assay has become a popular option to visualize DNA damages. This assay can either be used to assess the repair rate of the cells under study or to study the complexity of the induced damages and relate it with a dosimetric or microdosimetric quantity. This technique consists in tagging the repair proteins with fluorescent bio-markers to later be seen under fluorescence microscopy. The technique is addressed in section 3.2 in more details.

3.1 Clonogenic Assay

When one single cell can grow into a colony large enough that can be easily seen with the naked eye, we have a convenient proof that it has retained its proliferative capacity. First, we prepare into suspension cells from an actively growing stock culture by the use of trypsin. Trypsin is an enzyme that dissolves and loosens the cell membrane and causes the cell to round up and detach from the surface of the culture vessel.

Then, using a hemocytometer or an electronic counter, we count the number of cells per unit volume of the suspension. The cells are then seeded into a dish and incubated for 1 to 2 weeks, where they can divide and form colonies that can be seen with the naked eye once fixed and stained.

Ideally, one should see as many colonies as nominal cells that were seeded, however, due to reasons that lie in suboptimal growth medium or errors, uncertainties in counting or trauma of trypsinizations and handling, the number of colonies expected is usually less than the nominal. We define the term plating efficiency (PE) that indicates the percentage of cells seeded that grew into colonies as:

$$PE = \frac{\text{Number of colonies counted}}{\text{Number of colonies seeded}} \times 100\% \tag{3.1}$$

Following irradiation and incubation for 1 to 2 weeks, one can observe the following: (1) seeded single cells that are still single and have not divided; (2) cells that have completed a small number of divisions and form tiny abortive colonies; and (3) cells that have grown into large colonies and differ little from the unirradiated controls, i.e., cells that are said to have survived.

The surviving fraction (SF) is given by:

$$SF = \frac{\text{PE of irradiated}}{\text{PE of control}} \times 100\% \tag{3.2}$$

The procedure is repeated a number of times so each dish is exposed to a different dose and a curve of Survival Fraction vs dose can be plotted. The number of cells seeded per dish is important and must be adjusted in a way that it doesn't result in: (1) too few colonies and therefore the results are not statistically significant; (2) too many colonies that tend to merge, which makes the counting difficult and not accurate.

3.1.1 Survival Curves

A cell survival curve represents a relationship between radiation dose and the fraction of cells that survive the irradiation. The notion of a cell "surviving" the irradiation may have different meanings depending if we are referring to cells that proliferate or cells that do not proliferate. In the first case, where nerve,

muscle or secretory cells are included, “cell death” means the cell has lost its/a specific function. For proliferating cells (stem cells, for example), it is said the cell has not survived the irradiation if it has lost its reproductive integrity. One can see the cell physically present and even apparently intact, it can also be able to synthesize DNA, but if it cannot divide indefinitely, if it has lost that capacity, then the cell is considered dead. For non-proliferating cells, it is usually necessary to expose the cells to a dose of 100 Gy. Proliferating cells lose the proliferative capacity with a dose of less than 2 Gy. The dominant death mechanism following irradiation is mitotic death (death while attempting to divide) although some cells may also die from apoptosis (programmed cell death). The common experimental technique (clonogenic assay) and the survival curve, however, do not distinguish whether the cell died from mitotic or apoptotic deaths. As it was mentioned previously, the survival curve is obtained when one plots the SF versus dose, however, its shape depends on the type radiation used: sparsely ionizing (low LET), such as x- or γ-rays, or densely ionizing (high LET), such as α particles and neutrons. For the first group, in a linear-log plot, the survival curve starts as a straight line with a finite initial slope, revealing an exponential relationship between the quantities, and, at intermediate doses, it starts to bend, often described as a shoulder region. At higher doses, the survival curve becomes once again a nearly straight line. For hight LET radiations, in a semi-logarithmic plot, the curve is mostly a straight line for a wide range of doses. Figure 1 shows the difference between the two groups.

Through the years there were several mathematical methods developed, each with its degree of complexity, to describe the shape of cell survival curves, all having the same basic concept - the radiation's random number of energy deposition -, however, two descriptions have become widely known: the multitarget model and the linear quadratic model.

Multitarget Model

Widely used for many years, this model assumes the curve can be described with three terms: (1) a initial slope resulting from single-event killing; (2) a final slope resulting from multiple-event killing; (3) and a third term *n*, extrapolation number, that measures the width of the shoulder of the curve. D_0 and D_1 are the doses required to reduce the surviving fraction of cells to 37% of its previous value and are related to the final and initial slope, respectively. The curve is described as having a broad shoulder if *n* is large (e.g., 10 or 12) and a narrow shoulder if *n* is small (e.g., 1.5 to 2). Another way to measure the width of the shoulder is using the quasi-threshold dose D_q. Although there is no dose below which there is no effect produced by radiation and therefore no real threshold, D_q is a parameter that closely describes this concept and is related with *n* and D_0 by the expression (with *ln* as the natural logarithm) $ln(n) = D_q/D_0$.

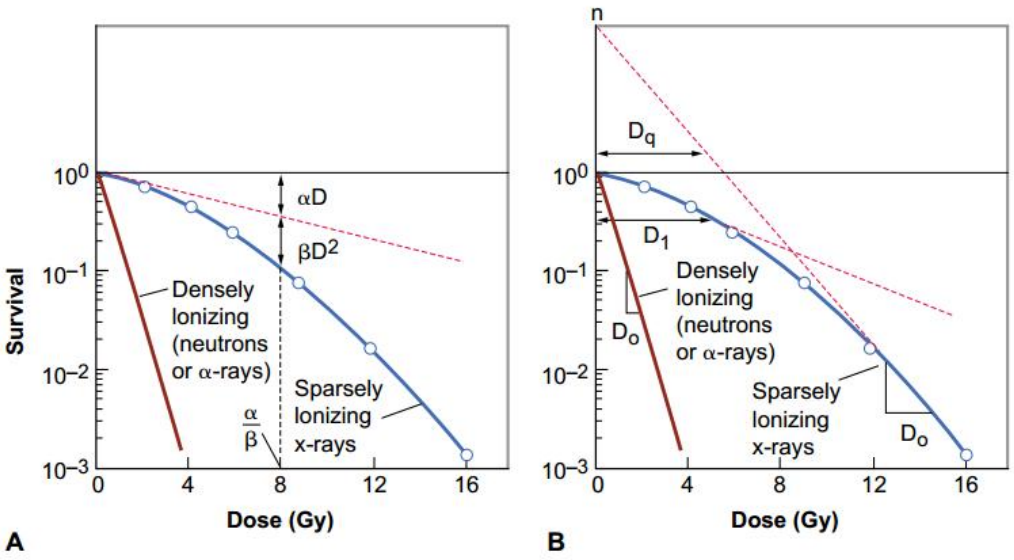

Figure 3.2: The shape of survival curves for mammalian cells exposed to high LET radiation (red line) and low LET radiation (blue line) with the surviving fraction (SF) plotted in a logarithmic scale and dose on a linear scale. (A) Linear Quadratic Model with the two components of cell killing - the linear (αD) and the quadratic (βD^2) - shown, as well as the dose at which those contributions are equal. (B) Multitarget Model described by an initial slope D_1, a final slope D_0 and n or D_q that represents the shoulder's width [7].

Linear Quadratic Model (LQM)

The linear quadric model is nowadays the most common used model to describe survival curves. In this model, we assume the cell killing by radiation has two components: one (α) proportional to dose and another (β) proportional to the squared dose. The second term introduces the concept of dual radiation action that was early studied in radiobiology, with chromosomes showing chromosome aberrations due to two separate breaks. In this model, the SF can be calculated with the expression (with α and β constants)

$$SF = e^{-\alpha D - \beta D^2} \tag{3.3}$$

When $\alpha D = \beta D^2$, which translated to dose means $D = \alpha/\beta$, it is said the linear and quadratic contributions to cell killing are equal. This model has, however, a problem: experimentally, at higher doses, the dose-response relationship is very much a straight line, revealing an exponential relation between cell killing and dose. In LQM, the curve is continuously bending and it doesn't fit experimental data at higher doses. Figure 3.2 shows the two different models just described.

3.2 Radiation-Induced Foci (RIF) Assay

The RIF assay is based on the knowledge that, following irradiation, specific signalling and repair proteins (common assayed proteins are γ-H2AX and 53BP1) start to localize to sites of DSBs in the cell's nucleus. The following paragraph briefly describes the assay using γ-H2AX.

The formation of DSBs is always followed by the phosphorylation of the histone H2AX, which results in the phosphorylated protein γ-H2AX. Since this event is initiated at a site of DSB, if the cell is incubated with a specific fluorescent antibody for γ-H2AX (which in turn is bound to a secondary fluorescent antibody), it will be possible to visualize a distinct focus under fluorescence microscopy. Although always questioned, some believe that there is a one-to-one correspondence between a DSBs and a γ-H2AX focus ([8], [9]), for this reason, the number of γ-H2AX foci can be seen as a measurement of the number of DSBs. The evolution of this number over time (for example, 30 minutes, 2, 6 and 24 hours after irradiation) reflects the kinetics of repair.

This assay starts by fixing the cells at a given time after irradiation, following by cell lysis. The cells are then incubated for 45 minutes to 1 hour with the first antibody and then, for the same amount of time, with the second antibody and mounted on a slide. A step-by-step description will be given in a later chapter.

3.3 Relative Biological Effectiveness

Talking about 1 Gy of neutrons and 1 Gy of x-rays is not the same thing. Although the dose is equal, the biological effect produced is different due to differences in the way each type of radiation deposits energy at the microscopic level. Therefore, in radiobiology, it is defined a quantity called Relative Biological Effectiveness (RBE). RBE represents a comparison between reference radiation (usually 250 kV x-rays or gamma-rays of Co-60) and test radiation and is calculated using the equation 3.4, where D_{ref} and D_{test} are the doses of reference and test radiations, respectively, that lead to the same biological effect.

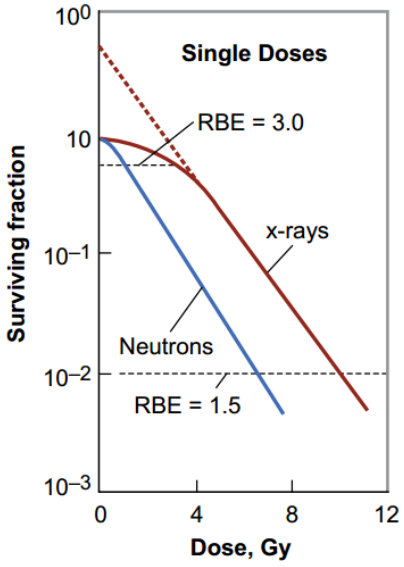

Figure 3.3: Cell survival curves for mammalian cells exposed to x-rays and fast neutrons showing the dependence of RBE on the choice of biological endpoint [7].

$$RBE = \frac{D_{ref}}{D_{test}} \tag{3.4}$$

One way to assess the RBE value is to realize a cell survival curve experiment with both the radiations. As it was briefly explained in the previous section, groups of cells are exposed to various doses of x-rays while parallel groups are also exposed to a range of doses of the test radiation and, in the end, the survival curves are obtained.

RBE, however, varies with many factors, such as LET, cell type and biological endpoint. As an example, we give the case presented in [7] for neutrons and x-rays (Figure 3.3). If we choose the biological endpoint as SF=0.01, the calculated RBE is equal to 1.5 (6.6 Gy for neutrons and 10 Gy for x-rays), but if the chosen endpoint is SF=0.6, the RBE is 3.0 (1 Gy of neutrons and 3 Gy of x-rays).

Chapter 4

Materials and Methods

For the present work, two different facilities were used for the irradiations of cells: Physikalisch-Technische Bundesanstalt (PTB), campus of Braunschweig, Germany and Centro de Ciências e Tecnologias Nucleares do Instituto Superior Técnico (C^2TN-IST) in Loures, Portugal. The first section of this chapter briefly describes the different irradiation facilities of both institutes. Subsections 4.2.1 and 4.2.2 explain in more detail the protocols for the Clonogenic and Radiation-Induced Foci Assays.
Irradiations for the first part of the work were carried out in June 2014, in PTB, by Prof. Dr. Ana Belchior within the framework of the European project BioQuart and the cell line used was HUVEC (Human Umbilical Vein Endothelial Cells).
Irradiation for the second part of the work were carried out between July and August 2018, in PTB, by João Canhoto and the cell line used was RWPE-1 (adult human prostatic epithelial cell lines).

4.1 Irradiation Facilities

4.1.1 Microbeam Irradiation at PTB

Following an ever-growing interested in microbeam irradiation due to the great advantages in studies related to the biological effects of radiations since the early years of the last decade [10], PTB started radiobiological experiments at its microbeam in 2002 [11]. The accelerator facility of PTB consists of a 2 MV Tandem accelerator and a cyclotron that can accelerate protons and α-particles up to 20 and 28 MeV, respectively. This range of particles and energies offers values of LET, in water, from 3 keV/μm up to 200 keV/μm.
The beamline (Figure 4.1) is 6.8 m long and 5 m tall, uses 2 electromagnetic quadrupole doublets and a beam defining aperture and slits to reduce the beam current to a few 1000 particles per second without compromising the spatial resolution.
In the basement floor, where the experimental area is situated (Figure 4.2), the cell dish is placed on a

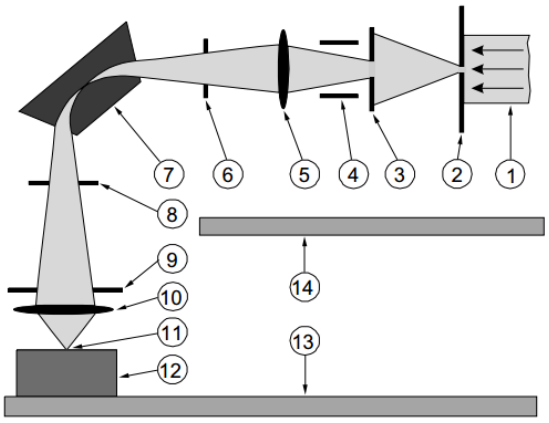

Figure 4.1: Sketch of the beamline and its components. 1. Incoming beam. 2. Object aperture. 3. Divergence slits. 4. Beam deflection plates. 5. Quadrupole doublet. 6. Slit. 7. Bending magnet. 8. Slit. 9. Anti-scatter-slit. 10. Quadrupole doublet. 11. Vacuum window. 12. Experimental area. 13. Basement floor. 14. First floor. [11].

xy-stage controlled by a computer and mounted on an inverse epifluorescence microscope. Below the microscope there is a CCD camera used to image cells, optimize the focus of the beam and to capture images for further analysis.

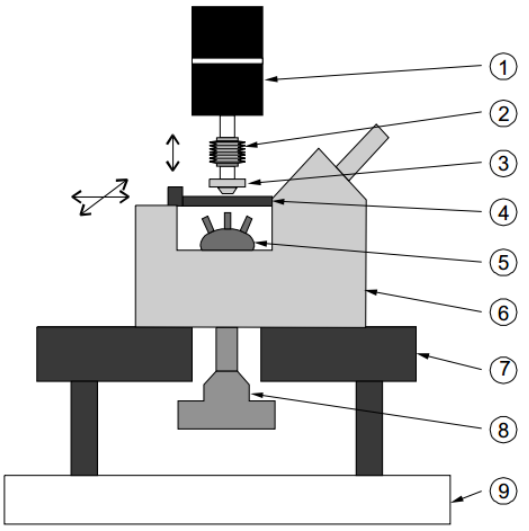

Figure 4.2: Sketch of the experimental area. 1. Quadrupole doublet. 2. Bellows for vertical-motor. 3. Vacuum window. 4. xy-stage. 5. Objective turret and detectors. 6. Inverse microscope. 7. Optical table. 8. CCD camera. 9. Basement floor. [11].

Because the beam has a downward direction, the cells must be plated in special cell dishes (Figure 4.3). The dish is made of medical steel with an inner diameter of 8 mm and one of the sides is covered with a special biofoil where the cells will be seeded in a drop and will adhere to the foil. The cell dish is then inserted into an aluminium ring which itself is fixed onto the *xy*-stage.

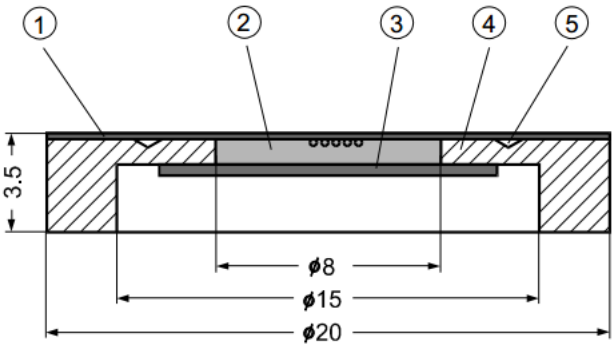

Figure 4.3: Sketch of the cell dish and supporting ring. 1. Cell-supporting foil. 2. Medium. 3. Cover glass. 4. Metal ring. 5. Groove. [11].

4.1.2 Americium-241 Irradiation at PTB

Besides the microbeam irradiation, there were also experiments carried out using an α-irradiator. This irradiator consists of a Am-241 source (whose nominal activity is of 195 kBq) mounted inside a vacuum system made of stainless steel. The irradiation port is sealed with a 2.5 μm-thick Mylar foil. For these irradiations, a 12.1 μm Myar foil [12] is glued to the bottom of the cell dishes. Between the two foils there is an air-filled safety gap of about 1mm.

4.1.3 Cobalt-60 Irradiation at C^{2}TN

Gamma irradiations for the experiments were carried out in Portugal, at the Radiation Technology Unity located at Centro de Ciências e Tecnologias Nucleares (C^{2}TN), a facility part of Instituto Superior Técnico. C^{2}TN possesses a Co-60 irradiation chamber - model Precisa 22, Graviner Lda, UK, 1971, [13] - comprising four retractable Cobalt-60 sources with a total activity of 150 TBq by June 2017. All irradiations were conducted at a dose rate of 1.18 Gy/min using only two sources. The dose rate at the irradiation position was determined using an ionization chamber before the experiment took place.

4.2 Protocols

In the first study, Human Umbilical Vein Endothelial Cells (HUVEC) were cultured in an incubator at 37°C in an atmosphere containing 5% CO_2 in EBM-2 (Endothelial Growth Basal medium), 4 to 5 days before irradiation to reach 90% confluence. For the second part of the work, non-cancerous cells from the human prostate (RWPE-1) were cultured in an incubator with the same temperature and CO_2 conditions in KSFM (Keratinocyte-serum free medium, ref no. 17005-034) supplemented with 10% FBS (Fetal Bovine Serum), 1% antibiotic, 0.05 mg/ml Bovine Pituitary Extract (ref no. 13028-014) and 5 ng/ml Epithelial Growth Factor (ref no. 10450-013) for the same time duration before irradiation to reach confluence level.

On the day before irradiation, a drop containing approximately 4000 cells was plated at the centre of each cell dish onto a Biofoil of 25 μm thickness.

For irradiations using the microbeam, on the day of irradiation, the cells were stained by adding the bisbenzimide Hoechst 33342 dye of a target concentration of 0.15 μM to the cells for 30 minutes. After that time, the cells were washed with fresh medium and remained in the incubator until the time of irradiation. Hoechst is a fluorescent dye (under excitation light, EL, of about 390 nm) that stains the nuclei and it is necessary for cell recognition before the irradiation on the microbeam. Since UV can also interact with the DNA molecules and create damages, all experiments carried out with the microbeam had not only irradiated and unirradiated (i.e., control) samples but also a third group of samples called SHAM. As is synthesized in Figure 4.4, irradiated samples are not only exposed to the desired radiation, but also exposed to the excitation light; SHAM samples are only exposed to EL; control samples are neither exposed to EL or radiation.

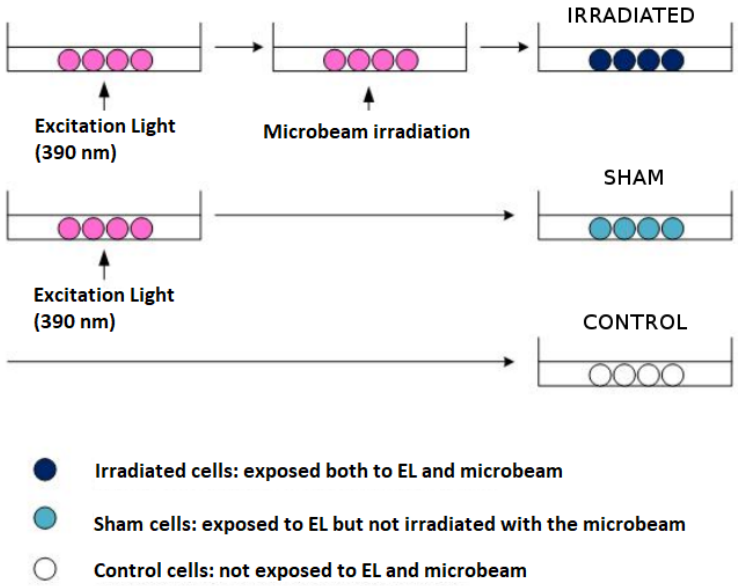

Figure 4.4: Experimental differences between the 3 sets of cell dishes: Cells that were exposed to both excitation light (EL) and microbeam are considered ”Irradiated Cells”, cells that were only exposed to eç are considered ”SHAM Cells” and cells that weren’t exposed to neither EL or microbeam are considered ”Control Cells”.

Cells were analysed at 64x magnificiation in an epifluorescence microscope. Image analysis of 53BP1 foci was performed using the free software Cellprofiler [14].

4.2.1 Clonogenic Assay

Co-60 Irradiation

For the γ-irradiation performed at C^2TN, cells were cultured in six-well plates prior to the irradiation. Each plate had a selected number of cells that depended on the nominal dose it would be exposed to. The

six-well plates were put inside the Co-60 irradiation chamber and were exposed to doses of 0.5, 1, 2, 4, 6 and 10 Gy. After irradiation, the six-well plates were placed inside the incubator (37°C and 5% CO_2) for 10 days so cells could grow and form colonies. Every two days the medium was changed. On the 10th day, the medium was removed and the six-well plates were washed with phosphate buffered saline (PBS), fixed with a solution of methanol and acetic acid in a ratio of 3:1 and stained with a 4% Giemsa solution.

Proton Irradiation

For proton irradiations, cells were exposed to cyclotron-accelerated protons (at PTB's microbeam facility) with an energy of 10 MeV at the entrance of the attached cells. The LET, in water, of the protons traversing the cell nuclei was approximately 4.7 keV/μm. Using data from previous irradiations ([15]), we could estimate that, for RWPE-1 cell nuclei with an approximated area of (167.1 ± 1.1) μm^2, the dose delivered to a nucleus by a single proton was about (4.3 ± 0.2) mGy. After irradiation, the cells were counted and a desired number of cells was plated in each well of each plate.

α-Irradiation

α-Irradiations were carried out at PTB with an Americium-241 α-source. Cells were exposed to 0.25, 0.5, 1, and 2 Gy at a dose rate of 43,5 mGy/min and a particle fluence of $(1.12 \pm 0.17) \times 10^7$ cm^{-2}. After irradiation, the cells were counted and a desired number of cells were plated in each well of each plate. For each dose, a total of 3 dishes were used.
Every two to three days the medium was changed. On the 10th day, the medium was removed and the cells were washed with phosphate buffered saline (PBS), fixed with a solution of methanol and acetic acid in a ratio of 3:1 and stained with a 4% Giemsa solution.

4.2.2 Radiation-Induced Foci (RIF) Assay

Immediately after irradiation, the cell dishes were placed in the incubator for the duration of the time-points assigned to each of them (either 0.5, 2, 4, 8 or 24 hours). When the incubation time was completed, the cell dishes were removed from the incubator and the cells were fixed with 4% formaldehyde in PBS for 15 minutes, at room temperature, followed by two rinses with PBS and permeabilization in 0.5% Triton X-100 lysis solution for 5 minutes. Cells were incubated for 1 hour at room temperature with primary antibody 53BP1 (rabbit polyclonal anti 53BP1, dilution 1:1000) diluted in PBS with 2% BSA. After this time, cells were rinsed with BSA (Bovine serum albumin) and then incubated for 1 hour with secondary antibody goat anti-rabbit (Texas Red-X, dilution 1:1000) diluted in PBS with 2% BSA. Again, after the stipulated time, cells were rinsed with BSA. All procedures took place on the cell dishes. Afterwards,

the circular section from the biofoil where the drop was placed was cut and mounted on a microscope slide with anti-fade ProLong Diamond (Invitrogen).

Chapter 5

Results and Discussion

5.1 Part One: Foci Analysis

In an experiment where the number of foci per nucleus is of interest, it is as or even more important to correctly identify what is a focus (and distinguish them between background foci and radiation-induced foci) from what is not. Although *CellProfiler* (CP) is a powerful tool for cell image analysis, it is only a first step and a help in identifying objects within a picture. Choosing the right parameters is always important but having a rigid pipeline (set of modules/tasks) could end up on losing important information. With this idea in mind, we analysed a couple of pictures to get an idea of the area of nuclei and foci, as well as the intensity of the latter, and to be able to set optimum upper and lower thresholds for area and a lower threshold for intensity, so that the software wouldn't try to identify artefacts that weren't clearly objects of interest and would make the analysis harder/impossible. The most important modules used where *ColorToGray* (to split the blue and red channel of the original picture: the blue channel contains essentially the information for nuclei and the red channel the information for foci, since nuclei are stained with DAPI, a blue fluorescent tag and foci with Texas-Red, a red fluorescent tag), *IdentifyPrimaryObjects* (twice – one for nuclei and another for foci), *MeasureObjectSize* and *MeasureObjectIntensity* (again twice of each), *RelateObjects* (to create a relationship between foci and nuclei. It will be explained later) and finally *ExportToSpreadsheet* (to save the data in CSV files).
Finally, for data cleaning, we wrote a R code, using the software Rstudio, to perform several cuts on the data based on parameters that will be explained throughout this chapter.

First Artefacts

The pipeline we created on *CellProfiler* starts by identifying the bigger objects that will be nuclei and then proceeds on identifying the small objects that will be foci. Within each picture, each big and small object are assigned a number starting from 1. Then it is possible to relate them to a parent/child

relationship. If CP identifies 5 small objects inside the boundaries of a bigger object, those five small objects are called child objects of the bigger one and, therefore, the bigger object is the parent object. We use this concept to perform the first cut on the output data from *CellProfiler*. Sometimes we can come across some artefact spots that retain some of the fluorescent stain (figure 5.1a). Since we can't relate these small objects to a bigger one (i.e., a nucleus), their Parent Object Number is zero (0). With no parent object, they are not useful for the analysis and therefore need to be removed from the pool of data. On R, they can be removed by identifying every line whose Parent Number column contains the value zero.

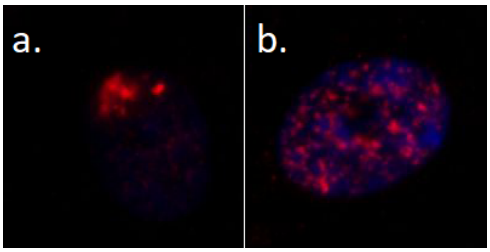

Figure 5.1: Example of artefacts that must be discarded: small objects with no parent objects (a) and cells with too many child objects (b).

Number of Foci per Nucleus

During irradiation, each nucleus was exposed to a near-UV light, for identification at the microbeam, and then 5 alpha particles, therefore, we expected to see only 5 foci per nucleus. However, due to handling, the near-UV light and other biological reasons, cells always show more foci then what is expected: these extra foci are called background foci. One of the assumptions on biological reasons to have more foci is that the cell was in division, where the amount of DNA is doubled (figure 5.1b). Because of this, we assumed that, for the analysis, SHAM cells couldn't have more than 10 foci and irradiated cells couldn't have more than 20 (up to 10 from irradiation plus up to 10 from background). Every SHAM and irradiated cell with more than 10 and 20 foci, respectively, was discarded.

Proximity to the border

Sometimes, nuclei get divided between picture frames, which means we can have a portion of a nucleus in one picture and the other portion on the following picture. This incident may create problems in the analysis, since, if not taken care of, the same nucleus will be identified twice. CellProfiler has an option to discard objects that touch the picture border, however, due to poor staining, CP sometimes manages to partially identify these nuclei. To overcome this problem, we implemented a process to select a "good area" within the image where we first retrieved the major axis length of each nucleus that remained from the previous cut (one of the output parameters we choose to determine on CP), then we took the average

and eliminated every object that was outside the region delimited by the following expressions, where (x,y) is the nucleus centre position, *l* is the average major axis length and 1016 and 896 are the numbers of pixels along the horizontal and vertical directions, respectively:

$$\begin{cases} l < x < 1016 - l \\ l < y < 896 - l \end{cases} \tag{5.1}$$

As it was previously said, it is of the utmost importance to correctly distinguish between background foci from radiation-induced (RI) foci and also distinguish foci from artefacts. During our first try at analysing the data, we noticed that our background data was not being well fitted by assuming a Poisson distribution, which resulted in a even poorer fit for the irradiation data. Since our goal was to obtain a good estimative for the probability of inducing a DNA damage, we needed to make sure that we had a good fitting model and parameters for the background (SHAM Irradiation). With this problem to solve, we changed the main focus of this part of the thesis and went back in our analysis to understand how could we get a better function to fit the background data and an improved background data set through filtering the observations by applying more thresholds to the data.

5.1.1 SHAM Frequency distribution: Poisson vs Exponential

Given the experiment, we would expect for the background to follow a Poisson distribution since the foci induced by the UV-light occur randomly in time. However, when observing the plot of relative frequency vs. number of foci per nucleus, the distribution had a shape much more resembling an Exponential rather than a Poisson distribution. At this point, it was important to understand what the best fitting distribution would be. With this idea in mind, we used the software Wolfram Mathematica to fit a Poisson distribution as well as an Exponential dependence to the data obtained from cell nuclei fulfilling the conditions in equation 5.1.

Both of the fit functions were evaluated based on the χ^2 Goodness of Fit Test, given by the equation 5.2, where N represents the maximum number of foci considered. As in our analysis we did not intend to analyse the likelihoods of obtaining observed values of χ^2 by applying a χ^2-Test, in equation 5.2, we used for O_n the observed relative frequency and for E_n the expected relative frequency, calculated using the fit function. (For an analysis of likelihoods, the absolute frequencies would have to be used in equation 5.2. The relevant χ^2 can be obtained by multiplying our χ^2 values by the number of cells considered in the analysis). In this test, a value close to zero indicates that the fit function closely reproduces the experimental data, while a value close to the expectation of the χ^2 distribution (equal to the ratio of maximum number of foci per cell plus one minus number of fit parameters and the number of cell nuclei considered in the analysis) indicates that the scatter of the data points with respect to the fit curve can be

explained by counting statistics. The results are presented in figure 5.2 and table 5.1.

$$\chi^2 = \sum_{n=0}^{N} \frac{(O_n - E_n)^2}{E_n} \tag{5.2}$$

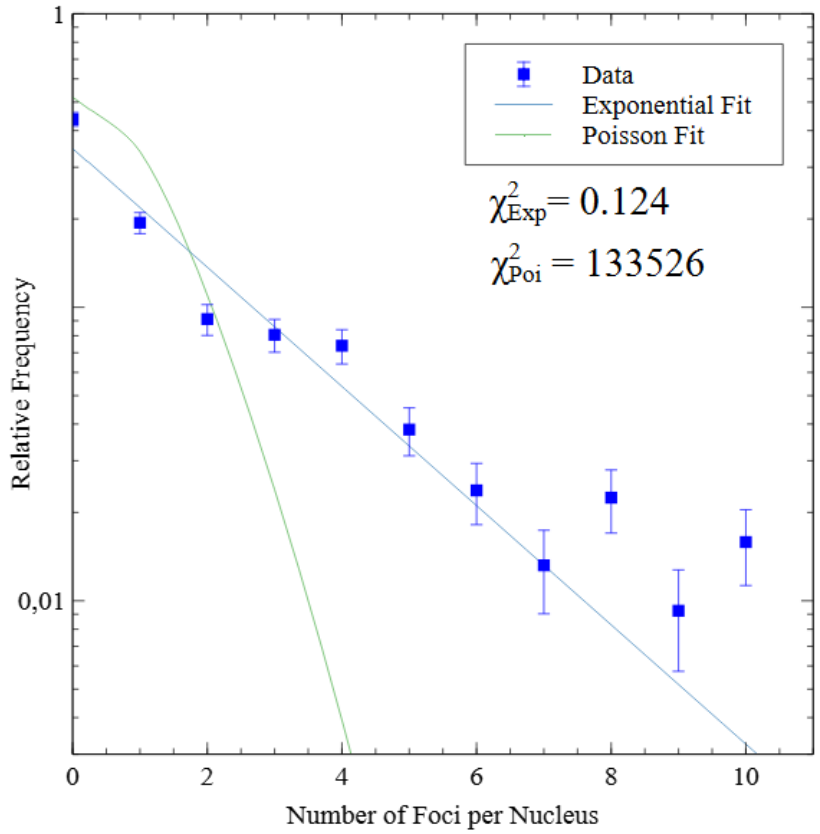

Figure 5.2: Exponential and Poisson fits to the frequency distribution when no thresholds are applied.

Analysing figure 5.2, where both fitting functions, as well as the experimental data, are plotted, and table 5.1, where the parameters and the respective standard errors (SE) are provided, it is possible to affirm that there is strong evidence to believe that the SHAM data follows an exponential decay, since the χ^2 value is much closer to zero for the exponential fit.

Even though the exponential decay was the function that best fit the data, it is also obvious, by looking at figure 5.2, that the distribution doesn't fit well the data, as the uncertainties lie outside the regression line for most points.

Table 5.1: Fitting parameters and respective standard errors (SE) for Poisson ($P_\lambda(x)$) and Exponential ($Exp(x)$) distributions.

Distributions	Parameters	
$P_\lambda(X = x) = e^\lambda \lambda^x / x!$	$\lambda = 0.65 \pm 0.16$	
$Exp(X = x) = ae^{-bx}$	$a = 0.35 \pm 0.04$	$b = 0.48 \pm 0.05$

5.1.2 Effects of parameters on the SHAM frequency distribution

Despite applying all the cuts mentioned and explained at the beginning of this chapter, by the end of the previous section, it became evident that although an exponential decay may seem the distribution of choice, the function poorly fitted the experimental data. This prompted us to believe that the data needed to go through a further step (or steps) in the cleaning process, specifically regarding the nuclei's area and the overall foci intensity. In the next sections, we describe two different studies/cuts performed and show the differences between the frequency distribution without thresholds, the best fit and two other randomly selected fits.

Once again, all the fitted functions were evaluated based on the χ^2 Goodness of Fit Test.

Foci Area x Intensity

We first turned our attention to an obvious parameter: the foci intensity. Analysing the images, we observed that sometimes the software identified small objects with low intensity as foci that clearly weren't what we were looking for. It became important to filter the data based on this parameter. CellProfiler gives as output a value of intensity for each object normalized to the area. Multiplying this value by the object's area, we get a quantity related to the overall intensity.

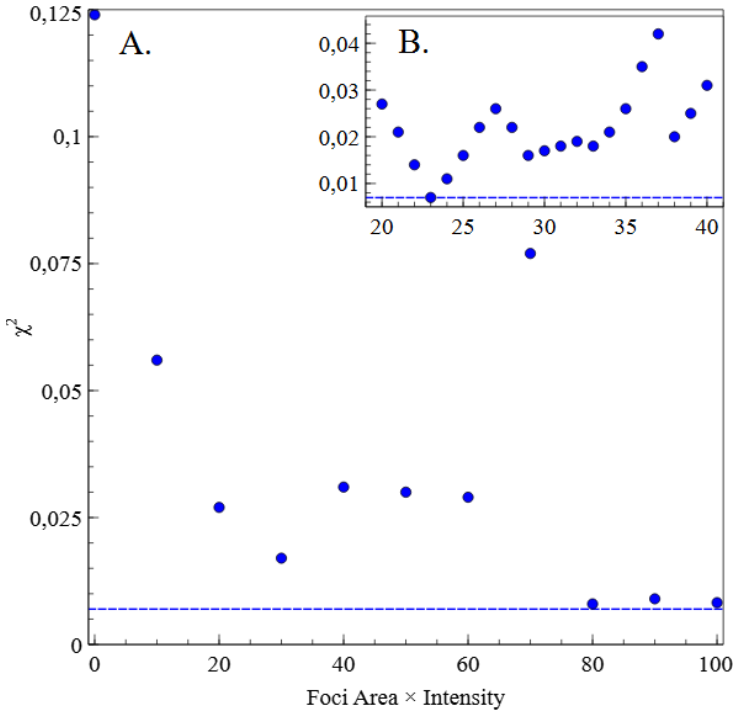

Figure 5.3: Variation of chi-squared depending on the threshold applied. (A.) from 0 to 100 in steps of 10 and (B.) from 20 to 40 in steps of 1. The dashed line represents the minimum value, corresponding to a threshold of 23.

Using the tools provided by Rstudio, we started to apply thresholds in steps of 10 beginning in zero (no threshold, for comparison purposes) and ending in 100. When performing this, we noted that for

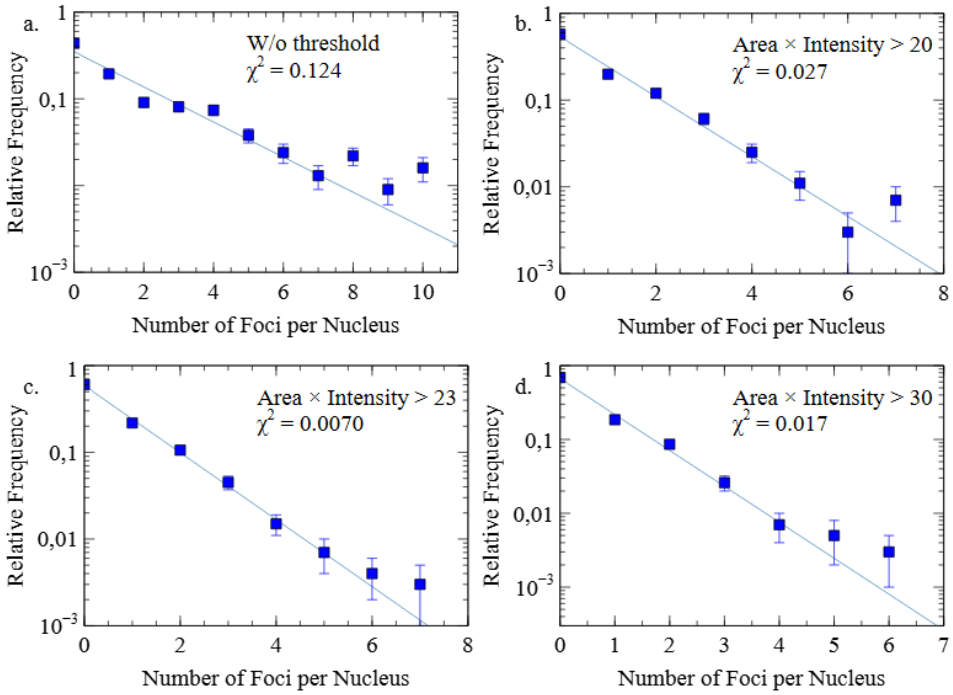

Figure 5.4: Study of the influence of the overall foci intensity (area x intensity) on the frequency distribution: only foci whose overall intensity was greater than 0 (a.), 20 (b.), 23 (c.) or 30 (d.) were considered.

a threshold equal or higher than 80, the number of points to fit was low (3 points), which means the probability to have a good fit is very high, so we did not value those results.

The results are shown in figure 5.3 A, and it is possible to see that there is a minimum value between 20 and 40, so we proceed on to redefine the step to 1 between 20 and 40 to look for the threshold value that would give us the lowest χ^2 and, therefore, the best fit. The results are shown in figure 5.3 B, where it is possible to see the minimum corresponds to a threshold of $Area \times Intensity = 23$. The dashed line represents this minimum value and it is plotted in both graphs for comparison purposes.

Figure 5.4 shows four different plots: the first plot represents the data and the respective fit and χ^2 value when no threshold is applied. The second, third and fourth represent the data when a threshold of 20, 23 and 30 is applied, with the respective χ^2 values. Comparing these values, we can see that the fit obtained after applying a threshold of 23 on the overall intensity shows a very good agreement with the experimental data.

Nuclei Area

Up to now, we haven't considered anything about the nuclei besides the maximum number of *children objects* (i.e., foci) and their centre position in the picture. In the previous section, we concluded that we should implement a threshold of 23 on the overall foci intensity. However, this was determined using every *parent object* that remained after the first triage. For foci, we previously mentioned that some

objects identified as *children objects* are not actual foci but rather some dirt present in the dishes, for example, and the same thing can happen to the *primary objects*. All these fake nuclei have one common factor - they have a small area -, which means that choosing a lower threshold for the nuclei area is necessary. It is also necessary to apply an upper threshold for one reason: during irradiation and then fixation of the cells, some cells had just finished division, which leads to at least two nuclei being close to each other. Sometimes they are so close, *CellProfiler* doesn't manage to identify them apart (*clumped objects*), resulting in an object with a larger area and possibly a high number of foci.

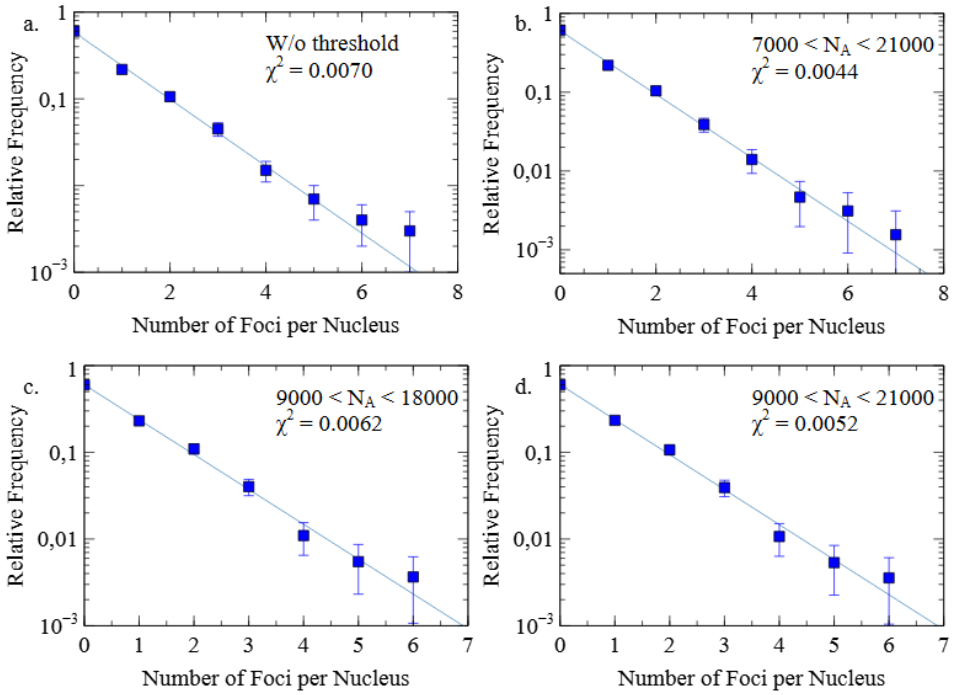

Figure 5.5: Study on how the lower and upper threshold on the Nuclei Area influence the outcome frequency plot and the respective exponential fit: (a.) No threshold applied on the nuclei area; only nuclei with area between 7000 and 21000 pxl^2 (b.), 9000 and 18000 pxl^2 (c.) and 9000 and 21000 pxl^2 (d.) considered.

Table 5.2: χ^2 values of the different thresholds applied to the nuclei area.

Case	χ^2
No threshold	0.0070
4000-16000	0.0150
7000-16000	0.0128
9000-16000	0.0105
4000-18000	0.0088
7000-18000	0.0055
9000-18000	0.0062
4000-21000	0.0077
7000-21000	**0.0044**
9000-21000	0.0052

In this section, we studied how different values for lower and upper thresholds would influence the

resulting frequency distribution and its exponential fit. We chose 3 different lower thresholds (4000, 7000 and 9000 pxl^2) and three different upper thresholds (16000, 18000 and 21000 pxl^2) by looking into the area distribution and what it felt like a good value. In figure 5.5 we show four different plots belonging to the case when there's no threshold applied, the best fit (7000-21000 pxl^2) and two other threshold cases. Comparing the chi-squared values given in table 5.2, we can see there are five cases where the fitting gets worse - all of which have a lower threshold of 4000 pxl^2 and the remaining two with the 16000 pxl^2 upper threshold -, in all other options, the fitting is better. The fit improves when compared to both the cases when we only apply a threshold on foci intensity and to the first exponential fit (shown in figure 5.2). We can now assume that the SHAM frequency distribution is well represent by the function

$$B(k) = ae^{-bk} \tag{5.3}$$

with $a = 0.60 \pm 0.02$, $b = 0.93 \pm 0.03$ and k represents the number of foci per nucleus.

5.1.3 Frequency distribution of irradiated cells

In the end, the real goal of the study is to analyse the damages induced by the radiation and be able to obtain a value representing the probability that a given ionising particle (with a given LET) will induce a focus in the cell nucleus. In the ideal world, our pool of data from the irradiated cells would only contain information about the foci induced by the ionising radiation of choice. However, that does not correspond to the truth. In the picture frames captured of the dishes that were irradiated we not only see foci that were induced by the radiation, but also what we already called background foci. Therefore, our data, $D(k)$, can be seen as a convolution between radiation-induced (RI) foci, $I(k)$, and background foci, $B(k)$, as described by the equation 5.4.

$$D(k) = \sum_{n=0}^{k} I(n) \times B(k-n) \tag{5.4}$$

This is another reason why the previous study is so important. In order to correctly identify the best expression and parameters for $I(k)$, we need to know or have a good estimative for $B(k)$, which we already have. So now, the challenge is to find an expression for $I(k)$ that when convoluted with $B(k)$ produces values that closely reproduce our real data.

As mentioned before, in the ideal world we would have $D(k) = I(k)$ and that is our starting point in "building" our function $I(k)$. Cells were exposed to 5 particles per nucleus in a given pattern (quincunx), therefore we would expect that $I(k)$ would take the form of a Binomial distribution of parameter *p* as presented in equation 5.5.

$$I(k) \equiv I(k;5,p) = \binom{5}{k} p^k (1-p)^{5-k} \tag{5.5}$$

There are, however, some incidents that can influence the resulting distribution. Those incidents are intrinsic to the microbeam itself and the software that runs and manages the microbeam and can result in the loss or addition of the number of particles to transverse the nucleus.

As previously mentioned, before irradiation, cells go through a recognition step where they are imaged with a near-UV light. Cells were incubated with Hoechst for a given time (30 min), however different cells show different levels of intensity under the near-UV light after that time. This can result in some cells not being identify by the software and, therefore, are not targeted by the radiation. However, after fixation, they are stained again, this time with DAPI. This second staining can turn weakly-stained nuclei into strongly-stained nuclei that can be recognised in *CellProfiller* and, if it is recognised, then we will have one unexposed nucleus presenting only background foci among exposed nuclei presenting both background and RI foci.

If the nucleus is "big" enough when comparing to the size parameters defined by the operator, we can have one nucleus being divided into two objects and being targeted twice which can result in having up to 10 RI foci in one single nucleus, i.e., an atypical situation that must be considered.

Although an assumingly much rare phenomenon, sometimes it can happen that 2 particles pass through the microbeam window, but the trigger registers only one event, giving rise to a higher number of particles in that specific nucleus.

These three incidents cannot be estimated by studying the SHAM cells and must be infer using the irradiated dishes. Leaving the last incident as a free parameter in our function $I(k)$, we analysed the annotated images to estimate values for the probability of a nucleus not being identified (p_0) or be targeted twice (p_{10}). Annotated images are pictures captured by the CCD camera and annotated by the software where one can distinguish between objects that were identified and presumably irradiated, objects that were identified but not irradiated and objects that were not identified due to poor staining but are clear nuclei that will probably be well stained in the end.

Based on these informations, we can now build our function $I(k)$ as:

$$I(k) = p_0\delta_{k0} + (1-p_0-p_6-p_{10})\binom{5}{k}p^k(1-p)^{5-k} + p_6\binom{6}{k}p^k(1-p)^{6-k} + p_{10}\binom{10}{k}p^k(1-p)^{10-k} \tag{5.6}$$

where $\delta_{k0} = 0$ for $k \neq 0$, $\binom{n}{k} = 0$ for $k > n$ and p and p_6 are the free parameters that represent the probability to induce a damage and the probability that two ions pass through the microbeam window at the same time, respectively. Based on our analysis of the annotated images, p_0 equals to 5.59% and p_{10}

equals to 1.33%

To find the best fitting parameters p and p_6, we wrote a C++ code that for each duplet (p, p_6) it would convolute $I(k)$ with the function $B(k)$ found in the last subsection and calculate the chi-squared value using the expression $\chi^2 = \sum_{n=0}^{N} \frac{(O_n - E_n)^2}{\sigma_n^2}$, σ_n being the uncertainty on each value. The fit with the duplet that results in the chi-squared (divided by the number of degrees of freedom ν) closer to one is considered the best fit to the data.

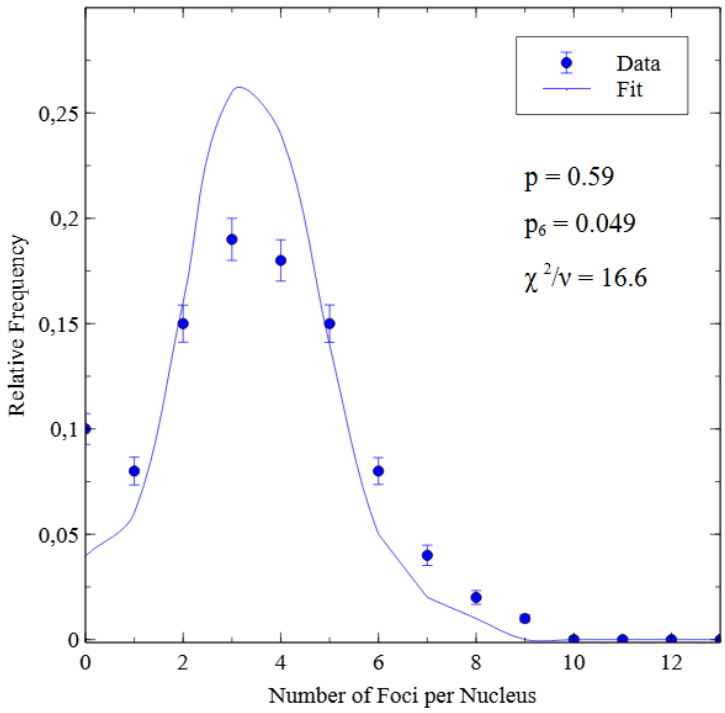

Figure 5.6: Data and best fit for the frequency distribution of foci per nucleus of cells exposed to 8 MeV alpha particles using the same thresholds used for the SHAM data (Foci intensity > 23 and Nuclei Area between 7000 and 21000).

Figure 5.6 shows the obtained frequency distribution of foci per nucleus of cells exposed to 8 MeV alpha-particles (blue circles) when we apply the same thresholds mentioned for SHAM and the function (blue line) that best fits our data based on the constrains $0 < p < 1$ and $p_6 < 0.05$ (as we expect this parameter to be lower than 5%). Both the data and the fit are zero for $k > 13$, therefore for better visualisation, the plot shows values for $k \leq 10$. As it is easily observed, although it represents the best fit, for most points the line lies outside the error bars, which indicates that $I(k)$ still doesn't reproduce our observed data. This made us believe that although a threshold of 23 for the overall foci intensity is the optimum value for SHAM, for some reason, it may not be the optimum value for the irradiated dishes. With this idea in mind, we applied three different and higher thresholds for this distribution. The results are shown in figure 5.7.

All distributions range from 0 to 20 Foci per Nucleus, but since for $k > 14$ the four distributions are zero, we plotted the distributions only for $k \leq 1$ for better visualisation and dotted lines are provided as

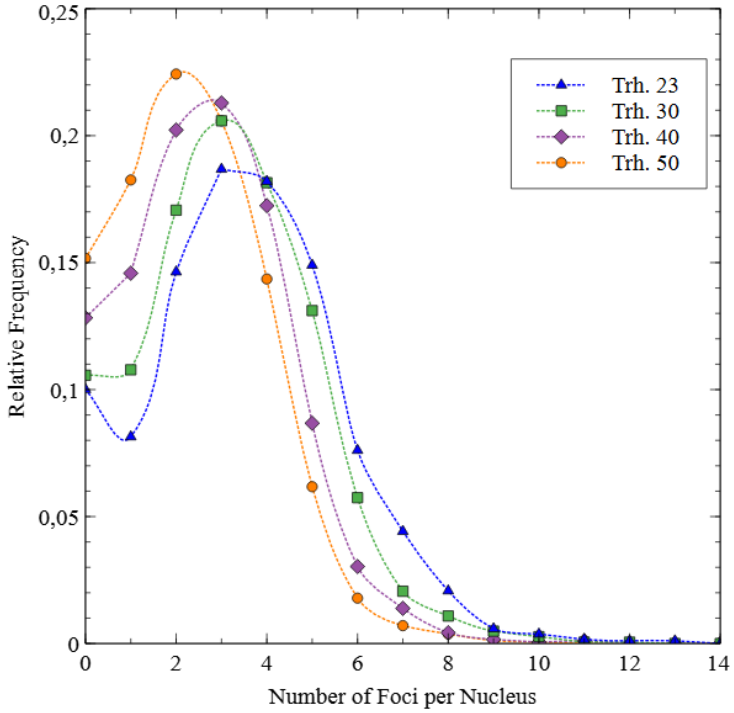

Figure 5.7: Frequency distributions of number of foci per nucleus of cells exposed to 8 MeV alpha-particles for different foci intensity thresholds (23, 30, 40 and 50). Dotted lines are provided as guides to the eye.

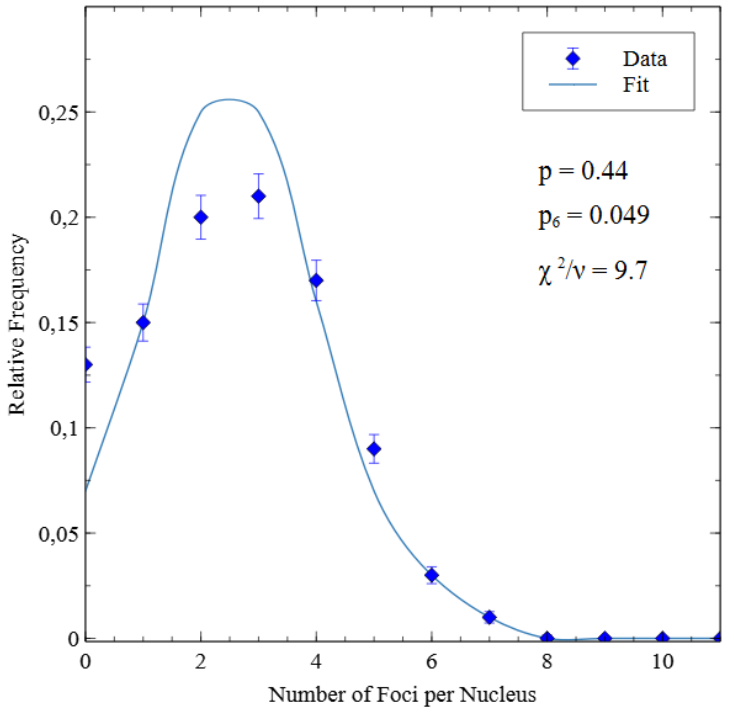

Figure 5.8: Data and best fit for the frequency distribution of foci per nucleus of cells exposed to 8 MeV alpha particles when the foci intensity threshold is increased to 40.

guides to the eye.

As we increase the threshold, the distribution starts to look like what we are expecting: an increasing from 0 to a number close to 5 (coincidently all distributions have a peak for $k = 3$, except the distribution

for a threshold of 50, that peaks at $k = 2$) and then a steep drop to zero for values higher than 5. Since the distribution with a threshold of 40 is the one that most closely resembles the expected distribution, we used it to, once again, find the best parameters of $I(k)$ (figure 5.8) and compare the chi-squared value with the one obtained for a threshold of 23. This time, we only plotted values for $k \leq 11$ since both the distribution and the fit are zero for greater values. Although for $k < 6$ the regression line lies outside the error bars for each point, comparing the chi-squared values, we see that the increase on the intensity threshold resulted in a new $I(k)$ with a smaller χ^2/ν, but still a far from one. This shows that there are still improvements to do regarding the cleaning of the pool of data of the irradiated cells.

5.2 Part Two: RBE of protons

One of the goals of this thesis was to study the behaviour of normal prostate cells to both γ- and proton-radiation and, in the end, estimate the RBE value for protons for this cell line. However, we faced problems with shipments, reagents, microbeam and cell cultures that made impossible to fully carry on the experiment until the end. With no possibility to repeat the experiment for the remaining time of the internship, we decided to use the Americium-241 source and perform a clonogenic assay for α-particles and calculate the RBE for this type of radiation. As described in the chapter Materials and Methods, cells were exposed to 0.25, 0.5, 1 and 2 Gy of α-particles, at a dose rate of about 43.5 mGy/min and to 0.5, 1, 2, 4, 6 and 10 Gy of photons at a dose rate of about 1.18 Gy/min.

The conventional protocol for clonogenic assays was performed on both experiments ten days after irradiation to evaluate the relative biological effectiveness (RBE) of α-particles. Figure 5.9 shows the survival fraction of RWPE-1 cells as a function of the mean absorbed dose for the two different types of radiation. Co-60 photons were used as the reference radiation.

For photon-irradiation, we obtained a curve (Figure 5.9, orange squares) with the expected shape for a sparsely ionizing radiation that could be fairly fitted with the linear quadratic (LQ) model (Figure 5.9, orange line), resulting in a α/β ratio of 76.7 ± 14.9 Gy. Based on our clonogenic assay study of RWPE-1 exposed to photons, we know that the platting efficiency (PE) of this cell line should be between 40%-60%, however when evaluating our results for the α-irradiation, two control culture wells were counted having 0 and 9 colonies, resulting in a PE of 0% and 18%, respectively. These values are extremely low and far from what was expected, clearly becoming outliers in our experiment and, therefore, were

Table 5.3: Fitted models (Linear Quadratic and Linear) and respective parameters

Model	Parameters	
$e^{-(\alpha_\gamma D+\beta_\gamma D^2)}$	$\alpha_\gamma = (0.47 \pm 0.01)$ Gy^{-1}	$\beta_\gamma = (0.006 \pm 0.001)$ Gy^{-2}
$e^{-\alpha D}$	$(\alpha = 1.13 \pm 0.02)$ Gy^{-1}	

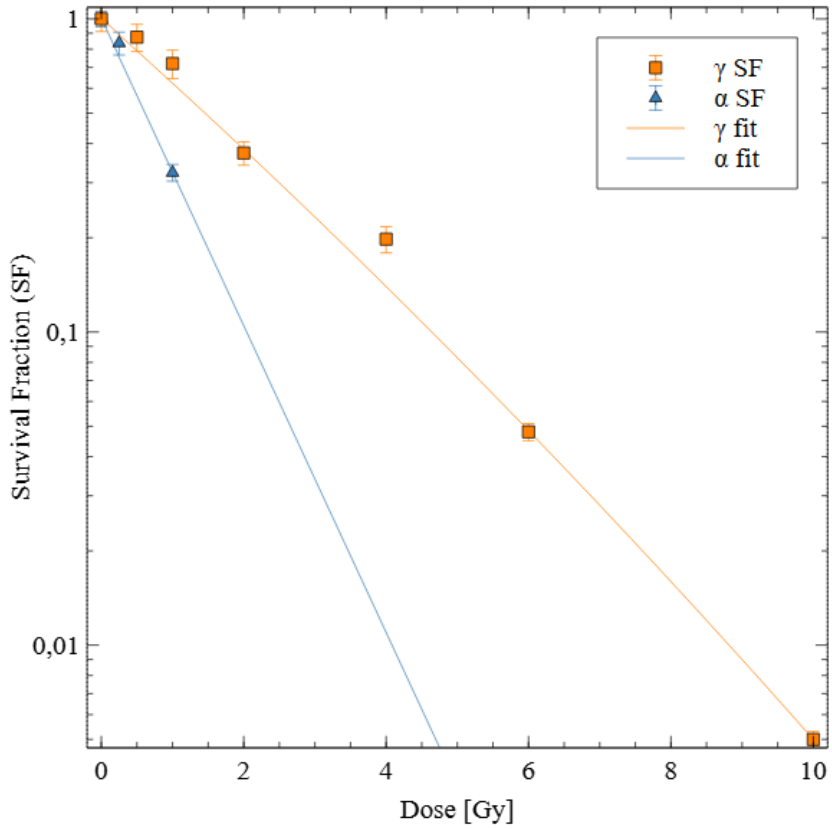

Figure 5.9: Dose-response curves for RWPE-1 exposed to Co-60 photons (orange) and Am-241 alpha particles (blue). Errors bars are standard errors.

not taken into consideration when calculating the PE for the α-irradiation. The culture wells with cells exposed to 2 Gy were also unusable due to signs of contamination and the culture wells of cells exposed to 0.5 Gy presented a Survival Fraction (SF) similar to the SF obtained for 1 Gy. Since this is not the expected behaviour and since the SF for 1 Gy was determined based on an average of 6 wells, we decided to drop the value for 0.5 Gy, using only the data from control (0 Gy), 0.25 and 1 Gy to plot the dose-response curve for α-particles (Figure 5.9, blue line and triangles). The curve shows the characteristic shape of high-LET radiations (as expected for Am-241 α-particles) that could be well fitted with a normal exponential decay (linear model). The parameter for this function, as well as the parameters of the LQ model used to fit the photon data, are presented in table 5.3.

As previously mentioned, the goal of this experiment is to determine the Relative Biological Effectiveness for the Am-241 α-particles. In Chapter 3, we mentioned that the RBE is calculated dividing the dose of photons by the dose of α-radiation that result in the same Survival Fraction (SF). Therefore, we have:

$$RBE(SF) = \frac{D_\gamma(SF_\gamma = SF)}{D_\alpha(SF_\alpha = SF)} \tag{5.7}$$

Since we have that

$$\begin{cases} SF_\gamma = e^{-(\alpha_\gamma D + \beta_\gamma D^2)} \\ SF_\alpha = e^{-\alpha D} \end{cases} \tag{5.8}$$

this results in

$$RBE(SF) = \frac{\alpha\left(\alpha_\gamma \pm \sqrt{\alpha_\gamma^2 - 4\beta_\gamma Log(SF)}\right)}{2\beta_\gamma Log(SF)} \tag{5.9}$$

With a quick use of a software like Wolfram Mathematica (WM), we conclude that the only valid function is when the square root follows a minus sign (SF ranges from 0 to 1 and RBE must always be positive). According to the consulted literature ([16], [17], [18]), a usual end-point considered to calculate the RBE is $SF = 0.10$. The obtained value for this end-point was 2.27 ± 0.06. This value is far from similar experiments who reported an RBE for Am-241 α-particles of 6.3 [16], a value close to 6.5 [19] or even a value of 14.6 [20]. However, these values were calculated using as reference radiation either Cs-137 photons or 120 kVp X-Rays. Not only these photons are less energetic than Co-60 photons (0.6617 MeV for Cs-137 photons as compared to an average of 1.253 MeV for Co-60), but there is also a reported difference of 7% [21] between Cs-137 and Co-60, for example. RBE also depends on LET, cell line and end-point, among others. For all these reasons, the values mentioned earlier cannot be really compared to the obtained RBE in a one-on-one comparison, since all of them used a different cell line. [19] also had a different irradiation protocol (*in vivo*). No data on RWPE-1 for Am-241 or other α-source was found. Although the previous factors are important and take a role in the difference observed, the major contribution to that difference may come from our experiment itself. For statistical purposes and significance, it is recommended to have at least three independent experiments, however, due to problems already mentioned, our data for α-irradiation is an average of one (not complete) experiment, which implies that we cannot infer statistically significant results.

Chapter 6

Conclusion and Future Work

Being able to establish a further relationship between biology and physics, in this case, the probability of inducing DNA damage with a dosimetric quantity related to the radiation of exposure (LET, for example) can be a great step forward in understanding the biological effects of radiation. Part of this thesis had the aim to go that further and be able to estimate the probability for 8, 10 and 20 MeV microbeam-α-particles, however, that wasn't possible to achieve for now. During our analysis, we showed that our SHAM frequency distribution followed a exponential decay rather than a Poisson distribution (figure 5.2), but we also noticed that the basic cleaning process for the background data was not enough, resulting in a poor fit and, consequently, a poor fit for the irradiated data. With this in mind, we made the cleaning process more complex by studying how different parameters can influence the outcoming frequency distribution and, therefore, the resulting fit function. More specifically, we first focused on the overall intensity of each focus (subsection 5.1.2) since faint artefacts were being identified as foci by CellProfiler. We first applied thresholds from 0 to 100 (in steps of 10) on the product intensity $\times$ area (= overall intensity; a threshold of 10 implies that every foci with an overall intensity below 10 are discarded) and compared the chi-squared values of each exponential fit to find which threshold would result in having a better fit (Figures 5.3 and 5.4). With the best threshold for the foci intensity selected, we then focused on finding upper and lower limits for the nuclei area, since very big objects (most probably two nuclei clumped together) and small objects (most probably some experimental artefacts) were also identified by the software. After choosing three upper and lower limits, we proceeded by pairing them up and evaluated the resulting fit (Figure 5.5). This study lead us to find that choosing a threshold for foci intensity of 23 and selecting only nucleus with an area in pxl^2 between 7000 and 21000 would result in a better fit. In fact, by comparing the chi-squared value of this fit (0.044) with the correspondent value when we performed a fit with no threshold (0.124), it was possibly to verify that the fit was improved. This is a remarkable improvement and showed the importance on choosing the right parameters when cleaning the data of background and undesired "garbage". The main and initial goal of this part was not achieved as we showed that

by applying the same thresholds for the irradiated nuclei the resulting fit was still not good (Figure 5.6). When we applied three different and higher values for this parameter (Figure 5.7), the frequency distribution started to take the expected look and the fit for one of those distributions (foci intensity $>$ 40) revealed a better agreement between the expected and observed values. Increasing the foci intensity threshold may be a first step in the solution. Future work will focus on understanding/discovering which new values should be used for those thresholds in order to obtain a reliable fit for the observed data. If we can manage to find those values, and assuming our function $I(k)$ correctly describes our experiment, we will then be able to estimate for each radiation the probability to induce a DNA damage and compare our values with a similar study done by IRSN and presented in [22].
As a side note, for the χ^2 statistics used in this thesis, one should use absolute frequencies. However, all χ^2 values presented here were calculated using relative frequencies and to obtained the real absolute value, one shall multiply the relative value by the total number of cells. Despite this, our conclusions are still valid. For the study of foci Intensity $\times$ Area threshold and for the irradiated data, the number of cells is the same for all thresholds, therefore the relative and the absolute values of χ^2 differ only by a factor and a comparison between relative values or between absolute values will give the same result. For the study of Nuclei Area threshold, the total number of cells changes depending on the applied threshold, but it was later verified that the threshold of 7000-21000 pxl^2 was still the best option if instead, we compared the absolute χ^2 values. Regarding the exponential fit, due to normalization constraints, the parameters a and b are not independent, however, for simplification purposes, we let them vary independently in this study.

In the second part of the thesis, we focused on assessing the Relative Biological Effectiveness (RBE) of protons, but again due to contaminations and problems in the laboratory, that was not possible. Since RBE also depends on the cell line, we decided to evaluate the RBE for alpha particles for our cell line by exposing RWPE-1 cells to Co-60 photons and Am-241 α-particles. The value obtained was of 2.27 ± 0.06, which is not close to the expected value and also not close to values reported on other works, although they used different cell lines and a different reference radiation. Our experiment has also gone through other problems that made impossible to have enough data to infer statistically significant results, which most probably explains the difference observed. For the future, we plan to use the same cell line, irradiating cells once again with protons and making it possible to evaluate the response of non-cancerous prostate cells to this type of radiation, since it is the most used radiation to treat prostate cancer. Concluding the assessment of RBE for Am-241 α-particles may also be in the plans for the future.

Although both of our main goals were not achieved, this thesis has shown a novel way of dealing with the data obtained by radiation-induced foci assays by basing the decision of counting or not a foci/nucleus on

parameters (intensity and area) intrinsic to those objects that may lead to new and important discoveries in radiation biology.

Bibliography

[1] H. Domenech. *Radiation Safety: Management and Programs*. Springer International Publishing, 2017. ISBN 978-3-319-42671-6.

[2] Particle therapy co-operative group. URL `https://www.ptcog.ch`. [Online; accessed 6-June-2018].

[3] Portugal prepara a introdução de novas terapias para o cancro com base em física de partículas. *República Portuguesa*, October 2017. URL `https://bit.ly/2JodgtT`. [Online; In Portuguese; accessed 6-June-2018].

[4] INTERNATIONAL ATOMIC ENERGY AGENCY. *Relative Biological Effectiveness in Ion Beam Therapy*. Number 461 in Technical Reports Series. INTERNATIONAL ATOMIC ENERGY AGENCY, 468.

[5] Basics of biological effects of ionizing radiation - Lecture, Module 1, IAEA. URL `https://slideplayer.com/slide/4681119/`. [Online; accessed 6-June-2018].

[6] S. Tabakov, F. Milano, S. Strand, C. Lewis, and P. Sprawls. *Encyclopaedia of Medical Physics - Volume I and II*. CRC Press, 2013. ISBN 978-1-4665-5550-1.

[7] E. J. Hall and A. J. Giaccia. *Radiobiology for the Radiologist*. LIPPINCOTT WILLIAMS & WILKINS, 7^{th} edition, 2012. ISBN:978-1608311934.

[8] O. A. Sedelnikova, E. P. Rogakou, I. G. Panyutin, and W. M. Bonner. Quantitative detection of (125)IdU-induced DNA double-strand breaks with gamma-H2AX antibody. *Radiation Research*, 158(4): 486–492, 2002.

[9] A. N. Ivashkevich, O. A. Martin, A. J. Smith, C. E. Redon, W. M. Bonner, R. F. Martin, , and P. N. Lobachevsky. gH2AX foci as a measure of DNA damage: a computational approach to automatic analysis. *Mutation Research*, 711(1-2): 49–60, 2011.

[10] M. Folkard, B. Vojnovic, K. M. Prise, and B. D. Michael. The application of charged-particle microbeams in radiobiology. *Nuclear Instruments and Methods in Physics Research Section B Beam Interactions with Materials and Atoms*, 188: 49–54, 2002.

[11] K.-D. Greif, H. J. Brede, D. Frankenberg, and U. Giesen. The PTB single ion microbeam for irradiation of living cells. *Nuclear Instruments and Methods in Physics Research Section B Beam Interactions with Materials and Atoms*, pages 505–512, May 2004.

[12] M. Unvericht-Yeboah, U. Giesen, and R. Kriehuber. Comparative gene expression analysis after exposure to 123i-iododeoxyuridine, γ- and α-radiation - potential biomarkers for the discrimination of radiation qualities. *Journal of Radiation Research*, 59: 411–429, 2018.

[13] J. Madureira, A. I. Pimenta, L. Popescu, A. Besleaga, M. I. Dias, P. M. Santos, R. Melo, I. C. Ferreira, S. C. Verde, and F. M. Margaça. Effects of gamma radiation on cork wastewater: Antioxidant activity and toxicity. *Chemosphere*, 169: 139–145, 2017.

[14] A. E. Carpenter, T. R. Jones, M. R. Lamprecht, C. Clarke, I. H. Kang, O. Friman, D. A. Guertin, J. H. Chang, R. A. Lindquist, J. Moffat, P. Golland, and D. M. Sabatini. CellProfiler: image analysis software for identifying and quantifying cell phenotypes. *Genome Biology*, October 2006.

[15] D. Frankenberg, K.-D. Greif, and U. Giesen. Radiation response of primary human skin fibroblasts and their bystander cells after exposure to counted particles at low and high LET. *Int. J. Radiat. Biol.*, 82, No.1: 59–67, 2006.

[16] L. A. Beaton, T. A. Burn, T. J. Stocki, V. Chauhan, and R. C. Wilkins. Development and characterization of an in vitro alpha radiation exposure system. *Physics in Medicine and Biology*, 56 (12): 3645–3658, June 2011.

[17] P. Thomas, B. Tracy, T. Ping, M. Wickstrom, N.Sidhu, and L. Hiebert. Relative biological effectiveness (RBE) of 210Po alpha-particles versus X-rays on lethality in bovine endothelial cells. *Int. J. Radiat. Biol.*, 79, No.2: 107–118, 2003.

[18] M. R. Raju, Y. Eisen, S. Carpenter, and W. C. Inkret. Radiobiology of α Particles: III. Cell Inactivation by α-Particle Traversals of the Cell Nucleus. *Radiation research*, 128: 204–209, 1991.

[19] R. W. Howell, M. T. Azure, V. R. Narra, and D. V. Rao. Relative Biological Effectiveness of Alpha-Particle Emitters In Vivo at Low Doses. *Radiation Research*, 137 (3): 352–360, March 1994.

[20] N. A. Franken, R. ten Cate, P. M. Krawczyk, J. Stap, J. Haveman, J. Aten, and G. W. Barendsen. Comparison of RBE values of high-LET α-particles for the induction of DNA-DSBs, chromosome aberrations and cell reproductive death. *Radiation Oncology*, 6:64, June 2011.

[21] K. K. Fu, T. L. Phillips, D. C. Heilbron, G. Ross, and L. J. Kane. Relative Biological Effectiveness of Low- and High-LET Radiotherapy Beams for Jejunal Crypt Cell Survival at Low Doses Per Fraction. *Radiology*, 132: 205–209, July 1979.

[22] C. Villagrasa, S. Meylan, G. Gonon, G. Gruel, U. Giesen, M. Bueno, and H. Rabus. Geant4-DNA simulation of DNA damage caused by direct and indirectradiation effects and comparison with biological data. *EPJ Web of Conferences*, 153: 04019, 2017.

[23] E. B. Podgorsak. *Radiation Oncology Physics - A Handbook for Teachers and Students*. IAEA, 2015. ISBN 92–0–107304–6.

[24] L. J. Kuo and L. Yang. γ-H2AX - A Novel Biomarker for DNA Double-strand Breaks. *in vivo*, 22: 305–310, May-June 2008.

[25] L. J. Kuo and L. Yang. γ-H2AX foci as a measure of DNA damage: A computational approach to automatic analysis. *Mutation Research/Fundamental and Molecular Mechanisms of Mutagenesis*, 711(1): 49–60, 2011.

[26] K.-D. Greif, H. J. Brede, D. Frankenberg, and U. Giesen. The PTB microbeam: a versatile instrument for radiobological research. *Radiation Protection Dosimetry*, 122: Issue 1–4: 313–315, December 2006.

[27] M. Siddiqi and E. Bothe. Single- and Double-Strand Break Formation in DNA Irradiation in Aquous Solution: Dependence on Dose and OH Radical Scavenger Concentration. *Radiation Research*, 112: 449–463, 1987.

[28] A. Lühr, C. von Neubeck, M. Krause, and E. G. C. Troost. Relative biological effectiveness in proton beam therapy - Current knowledge and future challenges. *Radiation Oncology*, 9: 35–41, 2018.

[29] R. Mohan, C. R. Peeler, F. Guan, L. Bronk, W. Cao, and D. R. Grosshans. Radiobiological issues in proton therapy. *Acta Oncologica*, 56: 1367–1373, 2017.

[30] J. E. Turner. *Atoms, Radiation, and Radiation Protection*. Wiley-VCH, 3rd edition, 2007. ISBN 978-3-527-40606-7.